Spiral structure in the inner parts of the Galactic System derived from the hydrogen emission at 21-cm wavelength

Schmidt, M.

SPIRAL STRUCTURE IN THE INNER PARTS OF THE GALACTIC SYSTEM DERIVED FROM THE HYDROGEN EMISSION AT 21 CM WAVE LENGTH

BY M. SCHMIDT

This paper contains a first attempt to determine the spiral structure of the inner parts of the Galactic System from the hydrogen emission at 21 cm wave length. The observational material consists of 215 drift curves at longitudes $l = 340°, 345° \ldots, 35°$ at frequency intervals of about 40 kc/s and 125 line profiles at longitudes $l = 340°, 342°.5 \ldots, 40°$ and latitudes $b = +2°.5, +0°.5, -1°.5, -3°.5, -5°.5$.

The distribution in latitude is used to separate at each frequency the contributions from the two points on the line of sight that have the same Doppler shift. Information on the linear distribution of hydrogen perpendicular to the galactic plane is obtained from the angular distribution at frequencies closely corresponding to the maximum radial velocity (Table 3, Figure 3). The thickness of the layer between the points where the hydrogen density has dropped to half the maximum density has a constant value of about 220 pc for $R > 3$ kpc. The measurements are corrected for antenna pattern and bandwidth of the receiver. In a preliminary separation of the two contributions the influence of the continuous galactic radiation field is estimated. Then the intensities are converted to optical depth. Corrections are applied for the dispersion of random cloud velocities. The final separation results in maximum hydrogen densities n_H and mean z co-ordinates $\bar{z}$ of the hydrogen layer at 808 points in the galactic plane (Table 9, Figures 6 and 7, Plate B).

Four or five arms are seen. The Orion arm and the Sagittarius arm may be traced to the far side of the System. Both are clearly trailing. Further arms may be distinguished tangent to the line of sight at $l = 6°$, $l = 359°$ and $l = 346°$.

1. *Introduction.*

In the present paper a first attempt is described to derive the distribution of neutral hydrogen in the inner parts of the Galactic System from the emission at 21 cm wave length. The previous attempt by LOHMANN [1]) from published 21-cm line profiles was largely arbitrary. KWEE, MULLER and WESTERHOUT [2]) found two secondary maxima in the rotational velocities which they attributed to spiral arms.

The main difficulty in deriving the distribution of hydrogen from 21-cm line profiles is the ambiguity in distance at each frequency. If V_g is the radial velocity of a hydrogen cloud in the galactic plane due to differential galactic rotation, R its distance to the centre of the Galactic System, $\omega(R)$ the angular rotational velocity, $R_\circ$ and $\omega_\circ$ the corresponding quantities near the sun, and $l' = l - 327°.5$ the angle between the hydrogen cloud and the centre, then

$$V_g = R_\circ \{\omega(R) - \omega_\circ\} \sin l'. \qquad (1)$$

It is possible to compute $\omega(R)$ from this equation for each value of the radial velocity V_g at each longitude l. If the angular velocity $\omega(R)$ is decreasing with increasing R, as it does according to *B.A.N.* No. 458, we may obtain R from $\omega(R)$. However, the line of sight contains two points with equal R if $R < R_\circ$. Therefore, the emission measured at a certain frequency consists of contributions from two points. The separation of these contributions is attempted in this investigation by studying the distribution of intensity with galactic latitude. The information needed about the linear distribution of hydrogen perpendicular to the galactic plane is obtained from the only point in the line profiles where no ambiguity exists, viz. at the maximum radial velocity. No assumptions are made concerning the position of the layer of hydrogen with respect to the galactic plane. The final result consists of

1. the z-distribution of hydrogen at various values of R (section 11).

2. the distribution of $\bar{z}$, the z-value of the centre of the hydrogen layer, over the galactic plane (section 12).

3. the distribution of n_H, the hydrogen density at $z = \bar{z}$, over the galactic plane (section 13).

As the reduction involves many steps and consecutive approximations, a block diagram is provided (Figure 4) to show the general plan.

2. *Measurements.*

Galactic co-ordinates based on the standard pole $\alpha = 12^h40^m$, $\delta = +28°$ (1900), are used throughout this investigation.

A total of 215 drift curves, crossing the galactic equator at 5° intervals in galactic longitude from $l = 340°$ to 35°, with fixed paraboloid and fixed frequency, was obtained with the Kootwijk receiver in December 1953, May 1954 and December 1954. The radial velocity corresponding to each drift curve was computed and corrected for the orbital motion of the earth and for the motion of the sun with respect to the local standard of rest. The time at which the galactic plane $b = 0°$ passed through the centre of the beam was computed for each drift curve, taking the time constant of the receiver into account.

A description of the receiver and the method for computing the radial velocities, and the intensity scale, is given by C. A. MULLER and G. WESTERHOUT [3]). The line profiles at 2°.5 intervals in l from $l = 340°$ to $l = 40°$, and at latitudes of approximately

[1]) W. LOHMANN, *Zs. f. Ap.* **35**, 90, 1954.

[2]) K. K. KWEE, C. A. MULLER and G. WESTERHOUT, *B.A.N.* **12**, 211 (No. 458), 1954.

[3]) *B.A.N.* **13**, 151 (No. 475, first paper), 1957.

$b = +2°.5$, $+0°.5$, $-1°.5$, $-3°.5$ and $-5°.5$ from the catalogue (Table 1 in the paper cited) have been used in this investigation. These profiles are obtained in groups along declination circles, with intervals of 10^m in right ascension, corresponding to about 2° in b. The declination circles in this region cut the galactic equator under a large angle, so that a change in right ascension is primarily a change in galactic latitude. In the further reduction all line profiles on the same declination circle have been assumed to represent the line profiles at a fixed longitude l corresponding to the point with $b \approx -1°.5$, where maximum intensities are found.

3. *Determination of distances.*

For any velocity V_g in a line profile at longitude l, the angular velocity $\omega(R)$ may be calculated from (1), taking $R_0 = 8.2$ kpc and $\omega_0 = 26.4$ km/sec. kpc. The value of R may be found from $\omega(R)$ by means of the rotation curve, given in *B.A.N.* No. 458, Figure 10. Some values of $\omega(R)$ are tabulated in Table 1.

TABLE 1

Angular velocity of rotation, $\omega(R)$, taken from *B.A.N.* No. 458

R kpc	$\omega(R)$ km/sec. kpc	R kpc	$\omega(R)$ km/sec. kpc
1.5	108.0	5.5	40.4
2.0	88.0	6.0	37.4
2.5	74.8	6.5	34.7
3.0	65.7	7.0	32.2
3.5	58.3	7.5	29.7
4.0	52.5	8.0	27.3
4.5	47.8	8.2	26.4
5.0	43.7		

The distance to the sun is either

$$r_1 = R_0 \cos l' - \sqrt{R^2 - R_m^2}, \quad \text{or} \quad r_2 = R_0 \cos l' + \sqrt{R^2 - R_m^2}, \tag{2}$$

where $R_m = R_0 \sin l'$. The values of r_1 and r_2 for $l = 340°.9$, $343°.4$, ... at 20 kc/s intervals are given in Table 9. The relation between frequency and radial velocity used here is 1 km/sec $= -4.735$ kc/s.

4. *Corrections for beamwidth and bandwidth.*

Corrections for beamwidth of the antenna are applied only one-dimensionally in the latitude direction, because the variation of intensity with latitude is much greater than with longitude. The antenna pattern was determined from observations on the sun, carried out by Mr H. VAN WOERDEN, and appeared to have a nearly gaussian form. The half-power width of the beam was 1°.9 in horizontal direction and 2°.7 in vertical direction. A determination by G. WESTERHOUT from measurements on the radio source Cas A confirmed these values (Figure 2 of the preceding article, p. 203). The pattern is assumed to have an elliptical form. For each drift curve the effective halfwidth A of the beam can then be obtained from the angle between the galactic equator and the vertical at the time of observation. Correcting the drift curves for the beamwidth A was somewhat difficult because the halfwidths [1]) of many observed drift curves exceeded A by only 50%. It was thought best to approximate the drift curve $h(b)$ by a gaussian curve $g(b)$ with the same halfwidth W. This part may be corrected rigorously and yields a gaussian curve $g'(b)$ with halfwidth $G = \sqrt{W^2 - A^2}$. The residual distribution $r(b) = h(b) - g(b)$ represents a minor part in most cases. By EDDINGTON's approximation the first-order correction of the residual is obtained with

$$r'(b) = r(b) - \frac{A^2}{11.1} \frac{\partial^2 r}{\partial b^2}, \tag{3}$$

where $r'(b)$ is the corrected residual distribution. The corrected drift curve $i(b)$ then is the sum of the two corrected components,

$$i(b) = g'(b) + r'(b).$$

The factor $\frac{i(b)}{h(b)}$ represents the correction factor to be applied to a measured intensity h. Plots of this factor against frequency were made at each longitude and latitude where a line profile was available. These line profiles were then corrected for beamwidth by multiplying the intensity h, read at each frequency, by the corresponding value of $\frac{i}{h}$. No corrections could be made at $l = 340°.9$ and $l = 343°.4$ for $R < 4$ kpc, because the intensities become very low and the latitude distribution very narrow.

The corrections for the bandwidth of the receiver, which is 37 kc/s, are not large and may be determined by a formula similar to (3)

$$I(f) = i(f) - 123 \frac{\partial^2 i}{\partial f^2}, \tag{4}$$

where f is the frequency in kc/s and $I(f)$ the line profile corrected for beamwidth and bandwidth. In practice the second derivative of i against f was replaced by the second difference $\Delta^2 i$ over an interval of 20 kc/s in frequency. The correction then becomes $-0.3\ \Delta^2 i$. The corrected line profiles are given in Figure 1.

[1]) The word halfwidth of a distribution function denotes in this paper the full width between the points where the function has dropped to half its maximum value. The halfwidth of the density distribution perpendicular to the galactic plane is also called the thickness of the layer.

FIGURE 1

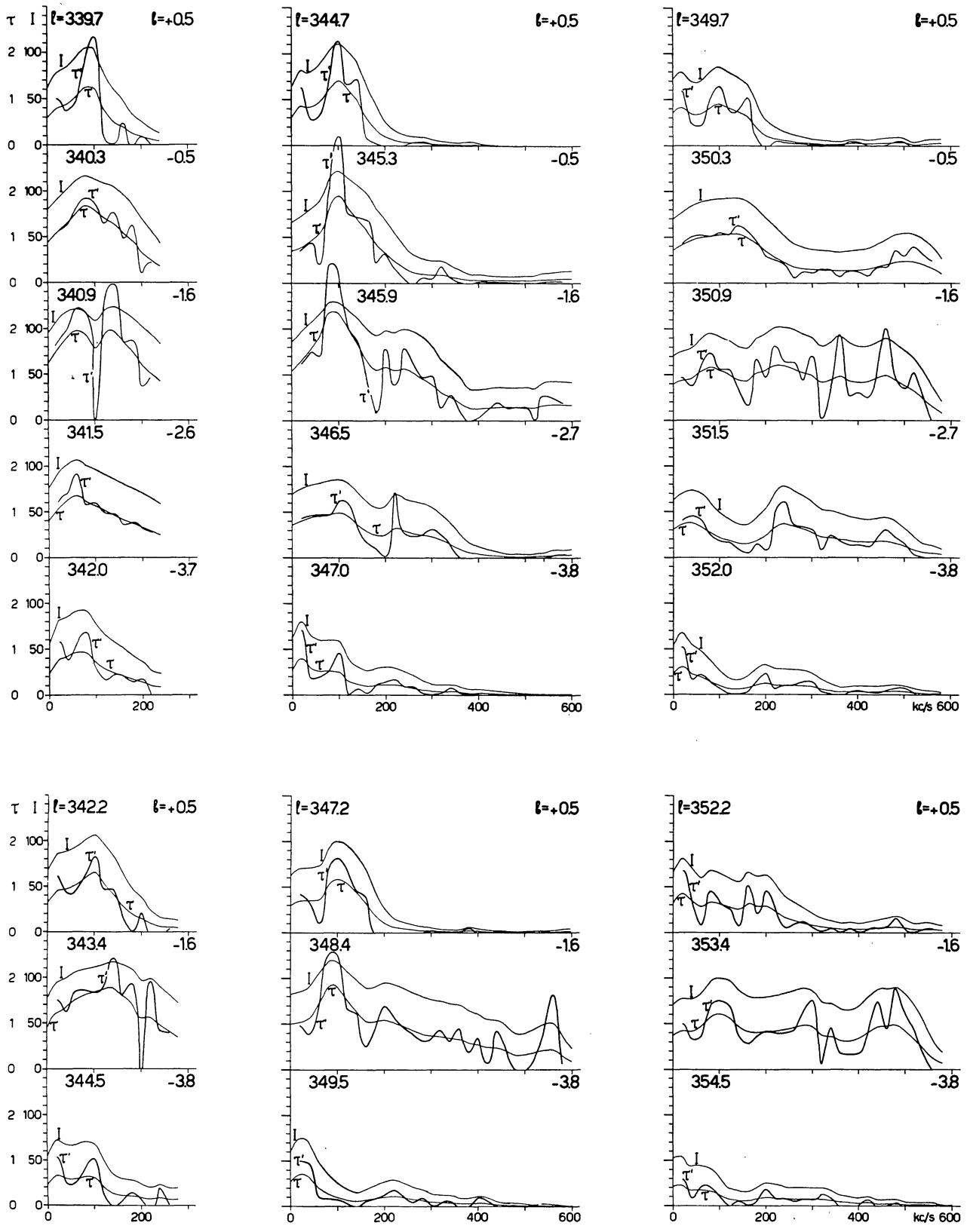

Line profiles corrected for bandwidth and antenna pattern (I), converted into optical depth (τ) and corrected for cloud velocities (τ′). Abscissae are kc/s, ordinates are intensities in mm on the record and optical depths.

FIGURE 1 (*continued*)

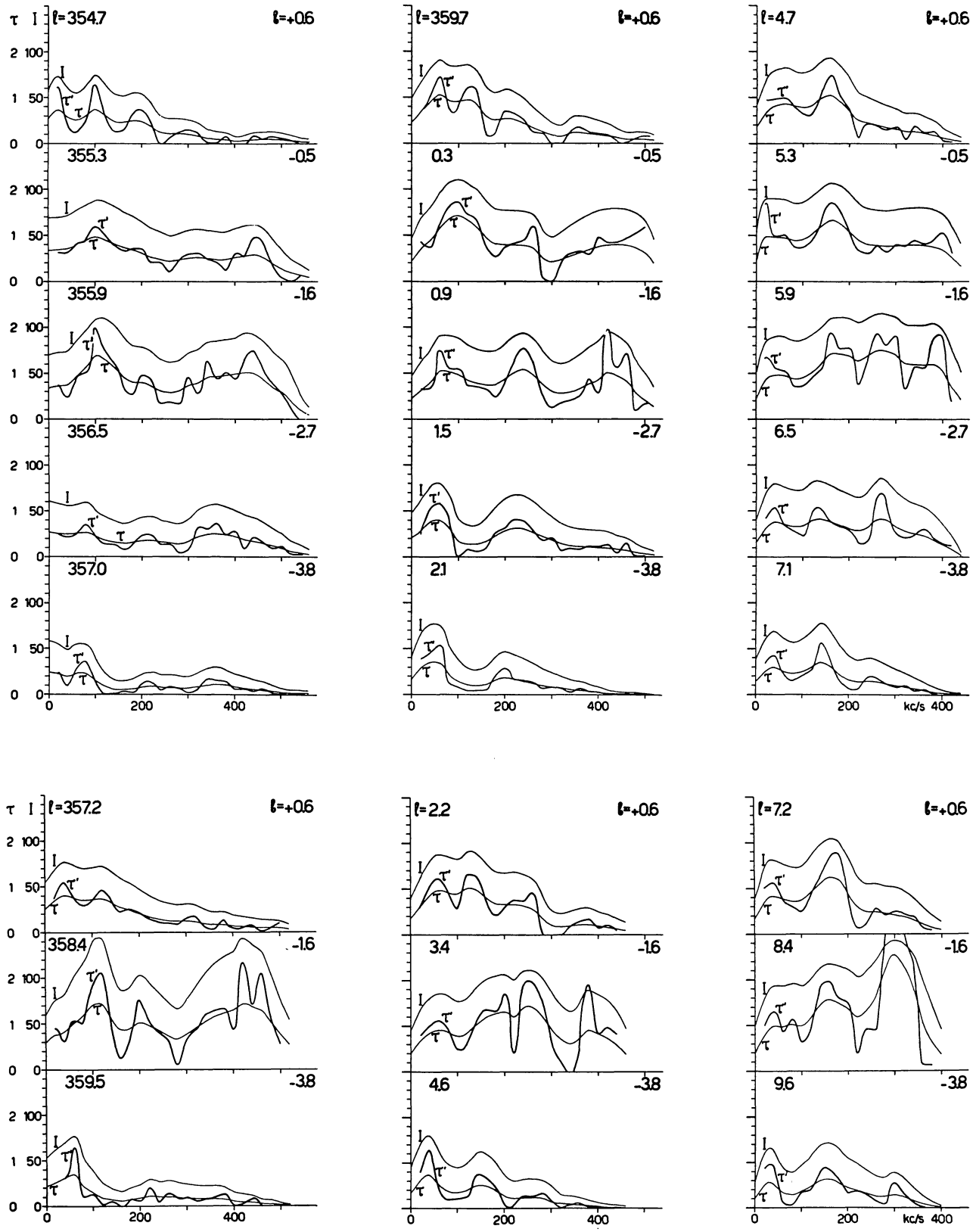

Line profiles corrected for bandwidth and antenna pattern (I), converted into optical depth (τ) and corrected for cloud velocities (τ′). Abscissae are kc/s, ordinates are intensities in mm on the record and optical depths.

FIGURE 1 (*continued*)

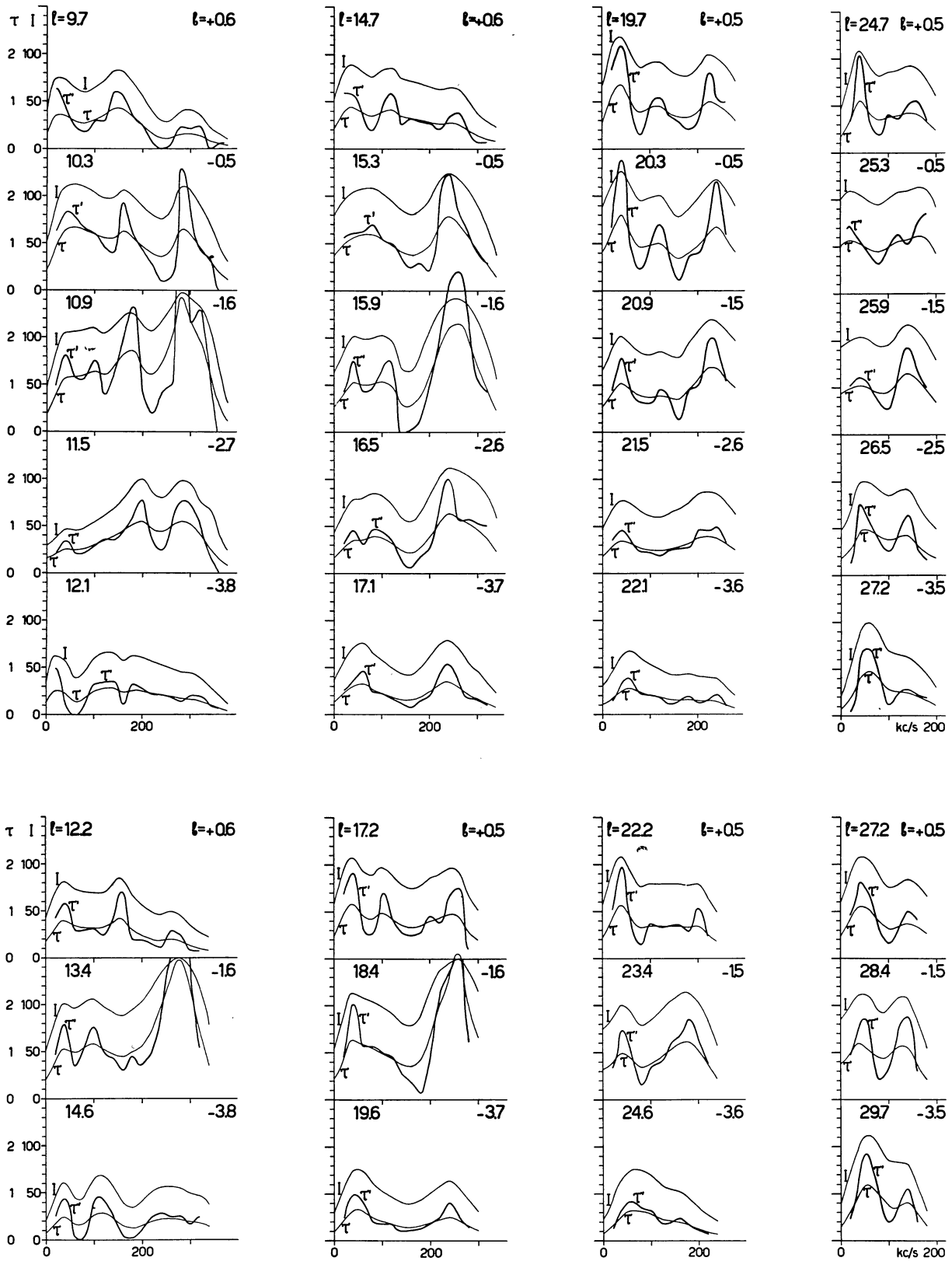

Line profiles corrected for bandwidth and antenna pattern (I), converted into optical depth (τ) and corrected for cloud velocities (τ'). Abscissae are kc/s, ordinates are intensities in mm on the record and optical depths.

FIGURE 1 (*continued*)

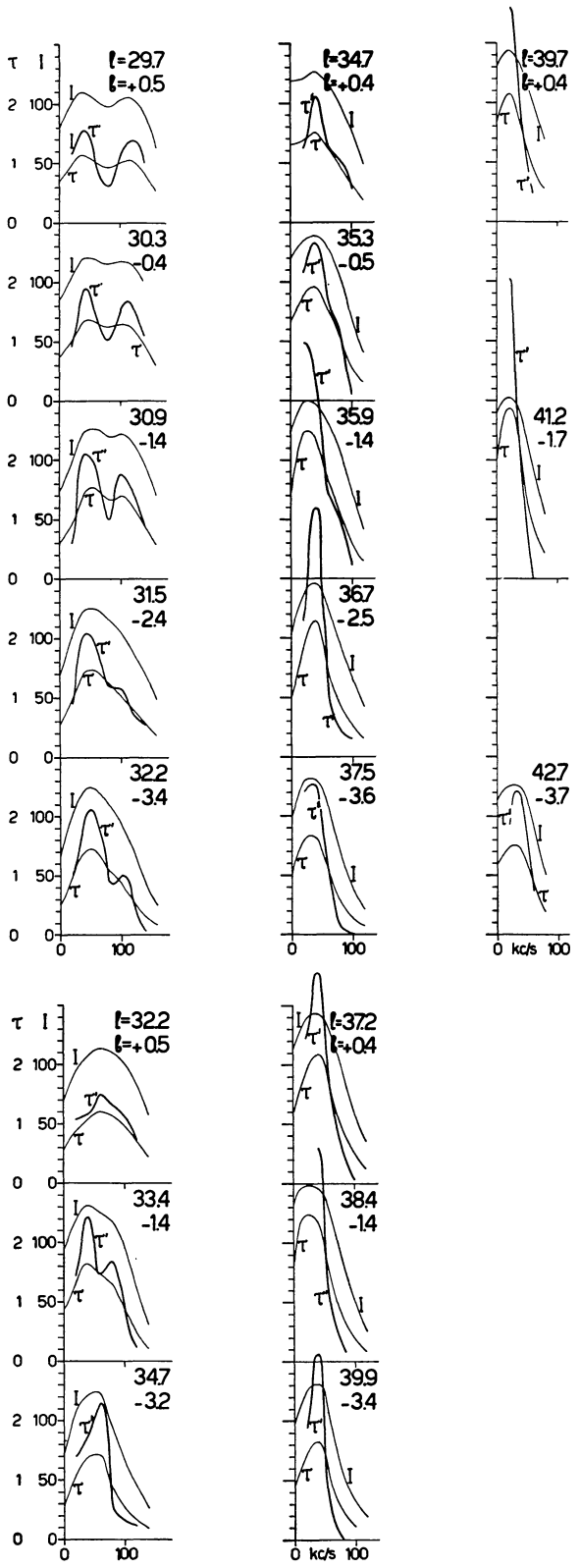

Line profiles corrected for bandwidth and antenna pattern (I), converted into optical depth (τ) and corrected for cloud velocities (τ'). Abscissae are kc/s, ordinates are intensities in mm on the record and optical depths.

5. *The space density of sources of continuous radiation.*

For the conversion of intensities into optical depths we need the distribution in space of the sources of continuous radiation. A preliminary investigation of the continuous radiation at 1420 Mc/s has been made by G. WESTERHOUT [1]). At the time when it became necessary to take the effect of the continuous radiation into account, there was little information about its distribution with longitude. Only one set of measurements, obtained by the author and reduced by WESTERHOUT, was available then. These measurements gave the intensity of the continuous radiation as a function of latitude for longitudes 340°, 350°, 0° and 10°, and have been used to obtain a rough idea about the distribution in space of the sources of continuous radiation. Later measurements have shown that the values at $l = 350°$ and $l = 0°$ both exceeded the values at neighbouring longitudes by more than 50 per cent, probably because they were taken in the neighbourhood of discrete sources. The unfortunate consequence is that the space density in degrees Kelvin per kpc of line of sight, given in Table 2 and used in this investigation, is wrong by more than 50%. The space model has been computed assuming axial symmetry of the radiation field.

TABLE 2

Space density of sources of continuous radiation, used in this investigation (superseded by later measurements).

b	R (kpc)					
	2	3	4	5	6	7
	source density (°K/kpc)					
+ 0°.6	0	0.6	1.3	2.1	1.7	0.4
− 0°.5	0	1.9	2.8	3.0	1.9	0.4
− 1°.6	0	3.0	2.8	2.4	1.3	0.4
− 2°.7	0	1.2	2.0	1.8	0.9	0.4
− 3°.8	0	1.1	1.1	0.7	0.6	0.2

For each longitude and distance the function I_{cr}, which is the intensity of the continuous radiation originating at distances greater than r was calculated from this model. The influence of the errors in this model on the final hydrogen densities is negligible. It is strongest in the densest parts, where it amounts to about 10%.

6. *Relation between observed line intensity, optical depth and continuous radiation.*

Let us consider measurements made at a frequency corresponding to the distances r_1 and r_2 ($r_1 > r_2$). Let I be the observed intensity in the line at this frequency, I_c the intensity of the continuous radiation in this direction and I_o the intensity for infinite optical depth. Further, let I_{cr_1} be the intensity of continuous radia-

[1]) *B.A.N.* **13**, 105 (No. 472), 1956.

tion from a distance greater than r_1, τ_1 the optical depth of the hydrogen at the distance r_1, and let I_{cr_2} and τ_2 be defined in a similar manner.

The intensity I is the difference between the combined intensities of line and continuum received in the measuring band and the intensity of the continuum received in the comparison band. The line intensity is

$$I_o(1 - e^{-\tau_1-\tau_2}).$$

The intensity of the continuum in the measuring band consists of a part $I_c - I_{cr_1}$, a part $I_{cr_1} - I_{cr_2}$ reduced by the hydrogen at r_1, and a part I_{cr_2} reduced by all the hydrogen. It is, therefore, in total

$$I_c - I_{cr_1} + (I_{cr_1} - I_{cr_2})\, e^{-\tau_1} + I_{cr_2} e^{-\tau_1-\tau_2}.$$

The intensity of the continuum in the comparison band is I_c. Hence, the measured intensity is

$$I = I_o(1 - e^{-\tau_1-\tau_2}) - I_{cr_1}(1 - e^{-\tau_1}) - I_{cr_2} e^{-\tau_1}(1 - e^{-\tau_2}). \quad (5)$$

The values of I_{cr_1} and I_{cr_2} may be computed from Table 2.

The value of I_o has been obtained by studying the maximum intensities measured in the direction of Cygnus through the Orion arm, in the direction of the centre and of the anticentre. The determination of I_o in the direction of Cygnus has been carried out in exactly the same manner as in *B.A.N.* No. 452 [1]). New observational data outside the galactic equator and corrected for antenna pattern gave $I_3 = 58°$ and $I_4 = 124°$, which then yielded $I_o = 126°$.

A second determination of I_o was made from the maximum intensity found near the galactic centre, corrected for continuous radiation. As all continuous radiation originates behind the hydrogen effectively observed, which is at a small distance owing to the lack of differential galactic rotation, the correction simply consists of adding the intensity of the continuous radiation to the measured line intensity. The maximum intensity found is 106° at $l = 329°.1$, $b = -2°.3$. The intensity of the continuous radiation is 17°. This continuous radiation, however, decreases the gain of the receiver by 2.8%, due to its effect on the automatic gain control [2]). Therefore the real line intensity I_o is $1.028 \times 106° + 17° = 126°$.

The agreement between both temperatures is better than could have been expected. In the direction of the anticentre a top intensity of 111° is measured. If the temperature is taken to be 126°, the optical depth in this direction should be about 2. This seems quite reasonable and does not contradict the assumed value of the temperature. It seems therefore that the temperature does not fluctuate very much in a large region of the Galactic System around the sun. In all reductions of 21-cm observations described in this series of papers the intensity of 125° for infinite optical depth has been used. A lower value does not seem possible but a somewhat higher value might also fit the observations.

[1]) H. C. VAN DE HULST, C. A. MULLER and J. H. OORT, *B.A.N.* **12**, 117 (No. 452, section 16), 1954.

[2]) C. A. MULLER and G. WESTERHOUT, *B.A.N.* **13**, 151 (No. 475, first paper, section 4), 1957.

7. *Preliminary determination of z-distribution of hydrogen at different values of R.*

We shall now determine the z-distribution of hydrogen from the latitude distribution near the maximum recession velocity for each longitude. The maximum recession velocity has been determined for all longitudes in *B.A.N.* No. 458. At this velocity, R reaches its minimum value $R_m = R_o \sin l'$, so that $r_1 = r_2 = R_o \cos l'$. These points are located on a circle having the line sun-centre as a diameter. We shall call this circle the midpoint circle. On this circle no ambiguity in distance exists and the angular latitude distribution of the intensity I may be converted into a linear z-distribution of optical depth τ. Only drift curves for which the frequencies are near the maximum radial velocity were used in the investigation of the z-distribution. It is sufficient then to put I_{cr_1} and I_{cr_2} equal to $\frac{1}{2} I_c$, so that

$$I = (I_o - \tfrac{1}{2} I_c)(1 - e^{-\tau}). \quad (6)$$

By means of this formula the optical depths were calculated from the intensities. Then τ was plotted

TABLE 3

Angle G between the latitudes where the hydrogen layer reaches half its maximum density, and corresponding thickness of the layer (see note on p. 248).

No. of measurement	l	G	Thickness
	°	°	
2271	345.9	1.20	161 pc
1747		1.17	157
2290	350.9	2.08	270
605		1.58	206
1344		1.84	240
592		2.03	262
1345		1.95	252
2336	355.9	1.84	229
1346		1.69	211
689		1.93	238
1347		1.89	233
2274	0.9	1.94	229
1348		1.77	208
2313	5.9	2.08	229
617		2.16	240
2275	10.9	1.97	200
618		2.03	210
2315	15.9	1.97	183
626		2.70	248
2335	20.9	3.66	307

FIGURE 2

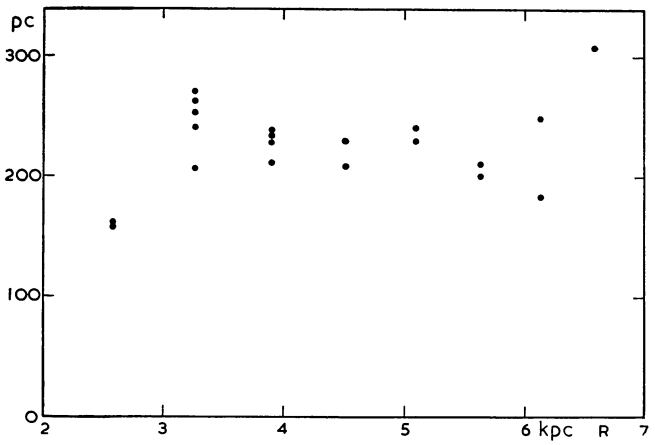

Thickness of the hydrogen layer between the points where the density has dropped to half the maximum density (not corrected for random cloud velocities).

against latitude b for longitudes 345°, 350°, . . ., 20°, and the angular halfwidth G of the latitude distribution was determined. This angular halfwidth was transformed to a linear halfwidth [1]) by means of the known distance $r_1 = r_2$. Here a small correction was applied in order to allow for the difference of the two distances r_1 and r_2. The resulting linear halfwidths are given in Table 3. They have been plotted against the galactocentric distance R in Figure 2. The scatter in the values of the linear halfwidth or thickness must be due, at least for a part, to irregularities in the z-distribution of hydrogen. The figure shows that the thickness hardly varies with R. A constant mean value of 230 pc was adopted at this stage of the reduction.

All graphs $\tau(b)$ were then reduced to halfwidth 2 and maximum value 1 and were plotted together with coinciding half-intensity points in Figure 3. The scatter in the points is not large. No systematic deviations depending on longitude were found. The gaussian curve with the same halfwidth is $e^{-0.693\,q^2}$ and is indicated by a few crosses in the figure. In the upper half the gaussian curve represents the distribution sufficiently well but in the outer parts the distribution is wider than the gaussian curve. The mean curve drawn through the points is tabulated in Table 4. We shall call this distribution $a(q)$ where $q = \frac{z - z_t}{115}$ and z_t is the z co-ordinate of maximum intensity.

Some asymmetry is indicated, the southern part being more extended than the northern part. An improved distribution is derived in section 11.

FIGURE 3

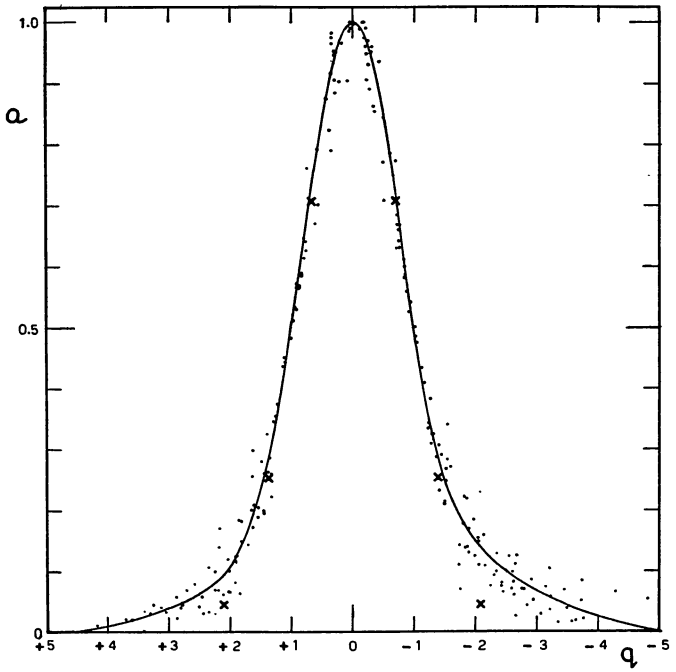

Distribution of hydrogen in the z-direction, normalized to $\tau_{max} = 1$ and halfwidth 2. Crosses indicate a gaussian curve with the same halfwidth.

TABLE 4

Distribution $a(q)$ of hydrogen in the z-direction; $q = \frac{z - z_t}{115}$. The finally adopted distribution $a(q)$ (cf. section 11) is symmetrical and identical with the values given below for $q < 0$, while $q = \frac{z - z_t}{110}$.

q	a $q>0$	a $q<0$	q	a $q>0$	a $q<0$
0	1.000	1.000	±2.5	.060	.100
±0.1	.993	.993	2.6	.055	.091
0.2	.972	.972	2.7	.050	.084
0.3	.940	.940	2.8	.046	.078
0.4	.895	.895	2.9	.043	.072
0.5	.841	.841	3.0	.040	.066
0.6	.779	.779	3.1	.036	.061
0.7	.712	.712	3.2	.033	.056
0.8	.642	.642	3.3	.030	.052
0.9	.570	.570	3.4	.026	.048
1.0	.500	.500	3.5	.023	.044
1.1	.432	.432	3.6	.020	.040
1.2	.369	.369	3.7	.018	.036
1.3	.316	.316	3.8	.015	.032
1.4	.270	.279	3.9	.012	.029
1.5	.230	.250	4.0	.010	.026
1.6	.199	.222	4.1	.008	.023
1.7	.169	.200	4.2	.006	.020
1.8	.145	.179	4.3	.004	.017
1.9	.126	.164	4.4	.002	.014
2.0	.110	.150	4.5	.000	.011
2.1	.096	.138	4.6	.000	.009
2.2	.086	.128	4.7	.000	.006
2.3	.076	.119	4.8	.000	.004
2.4	.068	.109	4.9	.000	.002

[1]) See note on p. 248.

FIGURE 4

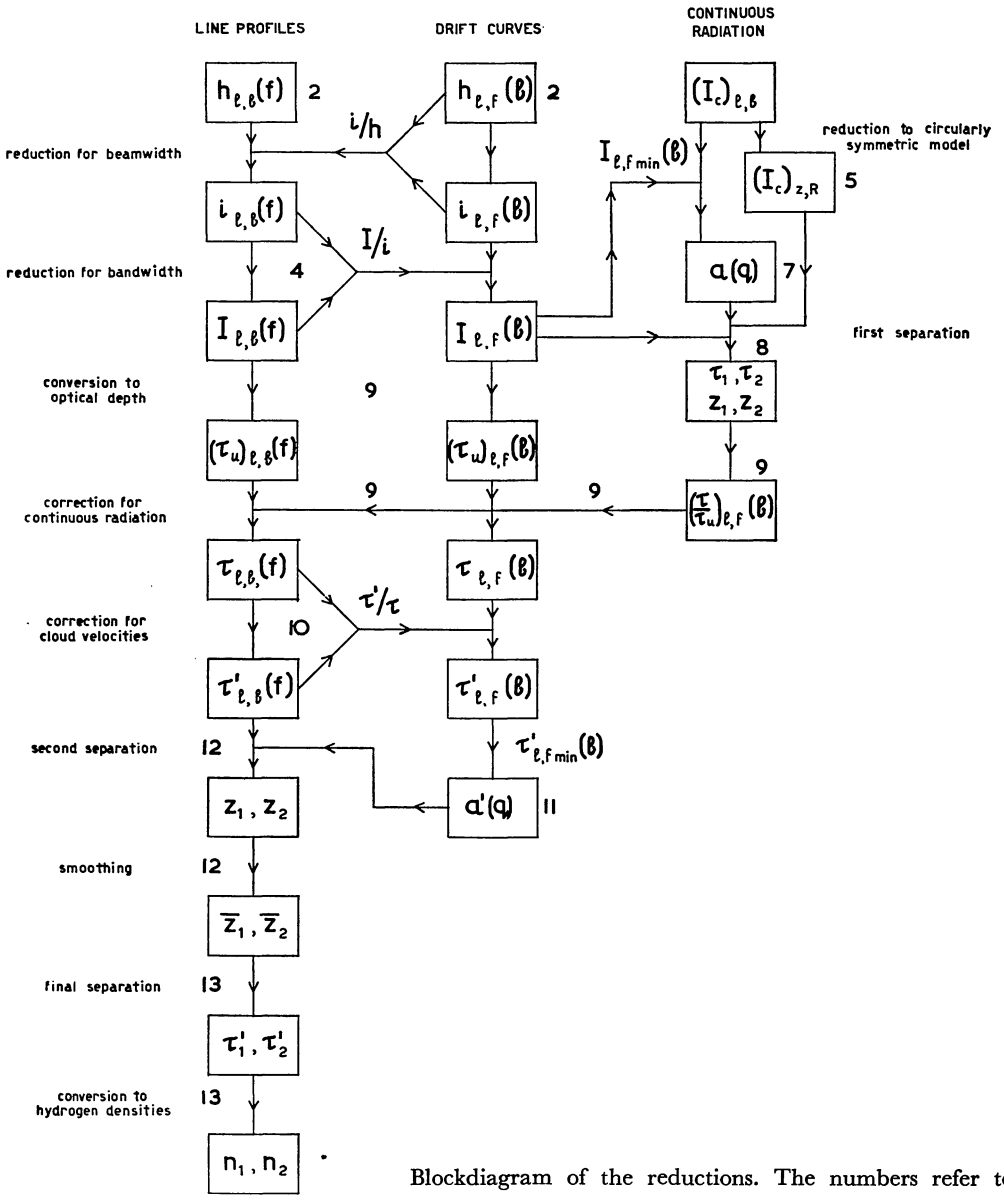

Blockdiagram of the reductions. The numbers refer to the sections.

8. *Preliminary separation of contributions from far and near points.*

The first separation (see blockdiagram, Figure 4) has to be carried out in intensities, because equation (5) does not allow a straightforward determination of total optical depth ($\tau = \tau_1 + \tau_2$) from the intensity I. It has been carried out for 118 drift curves as follows.

From the frequency at which a drift curve is observed, r_1 and r_2 are calculated by eq. (2). The distribution of optical depth with z at both these distances is assumed to have the form $a(q)$; it is transformed into angular distributions $a(b, b_t)$, where b_t is the latitude of maximum optical depth of one of the contributors so that $a = 1$ for $b = b_t$. Let the maximum optical depth be denoted by τ_t. The values of b_t and τ_t should now be determined for both contributors. Each drift curve should therefore yield four unknowns, which we shall call τ_1, τ_2, b_1, b_2. The total optical depth at any latitude b is

$$\tau_1 a_1(b, b_1) + \tau_2 a_2(b, b_2)$$

and the intensity read from the drift curve may be written by equation (5) as

$$I(b) = I_o(1 - e^{-a_1\tau_1 - a_2\tau_2}) - \\ - I_{cr_1}(1 - e^{-a_1\tau_1}) - I_{cr_2} e^{-a_1\tau_1}(1 - e^{-a_2\tau_2}). \qquad (7)$$

By reading the drift curve $I(b)$ at four different latitudes, we obtain four equations of the form (7) with four unknowns τ_1, τ_2, b_1, b_2. In principle the unknowns can thus be determined. In practice this

TABLE 5

First separation of drift curves into contributions at distances r_1 and r_2.

No. of measurement	f kc/s	R kpc	r_1 kpc	r_2 kpc	τ_1	τ_2	z_1 pc	z_2 pc
$l = 340°.9$								
1467	− 259	3.76	4.74	11.22	.42	.21	− 154	− 352
1466	219	4.19	4.25	11.71	.51	.50	105	346
1465	179	4.67	3.71	12.25	.84	.62	95	336
1432	145	5.17	3.17	12.79	.90	.96	74	325
1431	105	5.88	2.42	13.54	1.47	.83	31	− 146
835	− 55	6.96	1.28	14.68	1.06	.76	− 132	
$l = 345°.9$								
1712	− 420	3.34	5.67	9.89	.07	.24	− 135	− 237
1812	382	3.56	5.34	10.22	.14	.16	145	296
1836	382	3.56	5.34	10.22	.04	.27	172	329
1128	367	3.67	5.18	10.38	.08	.33	167	347
1694	342	3.83	4.96	10.60	.26	.24	152	323
1127	317	4.03	4.69	10.87	.25	.44	118	369
1820	302	4.15	4.54	11.02	.18	.65	137	358
1124	268	4.47	4.14	11.42	.13	.96	107	369
1689	263	4.51	4.09	11.47	.22	.94	92	385
1468	249	4.63	3.94	11.62	.26	.86	104	354
1807	223	4.88	3.64	11.92	.35	.76	95	342
1121	218	4.93	3.59	11.97	.52	.66	102	342
1798	183	5.35	3.10	12.46	.53	.61	54	304
1118	169	5.54	2.88	12.68	.68	.60	− 43	250
1110	110	6.38	1.95	13.61	1.30	1.32	+ 25	310
821	− 51	7.36	0.89	14.67	.90	.91	+ 8	− 366
$l = 350°.9$								
1357	− 442	3.78	5.62	9.44	.42	.49	− 175	− 259
1358	402	4.01	5.19	9.87	.35	.50	141	270
1370	361	4.28	4.76	10.30	.20	.74	153	289
1371	321	4.58	4.31	10.75	.33	.58	132	345
1372	281	4.88	3.90	11.16	.34	.72	136	355
1385	239	5.27	3.39	11.67	.38	.89	101	386
580	239	5.27	3.39	11.67	.24	.98	132	384
1386	199	5.68	2.88	12.18	.41	.68	76	355
686	159	6.13	2.34	12.72	.46	.72	− 5	220
1399	157	6.15	2.32	12.74	.58	.62	+ 3	186
622	120	6.61	1.78	13.28	.60	.68	29	218
616	78	7.19	1.12	13.94	.70	.71	31	279
575	64	7.36	0.94	14.12	.52	.54	32	310
698	61	7.40	0.89	14.17	.60	.54	+ 37	365
768	58	7.44	0.84	14.22	.60	.59	− 7	268
1415	− 35	7.74	0.51	14.55	.75	.27	+ 31	− 332
$l = 355°.9$								
1359	− 408	4.43	5.12	9.32	.72	.28	− 136	− 267
2302	402	4.47	5.04	9.40	.76	.24	132	256
1360	368	4.67	4.65	9.79	.63	.30	143	260
1374	327	4.95	4.17	10.27	.63	.20	120	294
2303	322	4.98	4.12	10.32	.57	.24	109	277
1373	287	5.26	3.69	10.75	.46	.22	87	271
1387	245	5.62	3.17	11.27	.43	.23	69	273
1388	205	5.98	2.69	11.75	.46	.36	− 38	310
1400	164	6.40	2.15	12.29	.33	.69	+ 3	312
687	157	6.47	2.06	12.38	.44	.72	14	266
1401	124	6.83	1.61	12.83	.50	.94	51	325
2273	115	6.93	1.49	12.95	.53	.96	9	300
1402	84	7.29	1.06	13.38	.56	.70	14	323
699	59	7.55	0.76	13.68	.50	.46	12	304
781	55	7.60	0.62	13.82	.63	.43	48	296
1416	− 32	7.85	0.41	14.03	1.11	.34	+ 122	− 366
$l = 0°.9$								
1349	− 375	4.96	4.79	8.91	.46	.50	− 97	− 167
1361	334	5.24	4.18	9.52	.45	.24	89	200
1362	294	5.54	3.62	10.07	.59	.07	102	278
581	283	5.63	3.48	10.22	.46	.26	91	310
1375	262	5.78	3.24	10.46	.66	.30	89	267
631	259	5.81	3.19	10.51	.74	.22	83	246
1389	221	6.12	2.71	10.99	.66	.36	75	258
1403	179	6.49	2.18	11.52	.48	.30	48	288
2324	174	6.53	2.13	11.57	.55	.54	− 21	202
1404	139	6.87	1.67	12.03	.60	.68	+ 21	178
1418	97	7.29	1.12	12.58	.64	.82	+ 39	160
809	77	7.47	0.90	12.80	.67	.58	− 15	207
828	− 64	7.59	0.75	12.95	.78	.45	− 10	− 198
$l = 5°.9$								
556[b]	− 360	5.35	4.78	8.08	.80	.44	− 113	− 194
556[a]	359	5.36	4.75	8.11	.69	.54	124	197
624	355	5.39	4.66	8.20	.64	.66	112	196
2292	315	5.66	3.95	8.91	.68	.63	95	230
632	303	5.74	3.78	9.08	.69	.74	94	236
633	277	5.91	3.43	9.43	.66	.78	80	285
641	239	6.20	2.82	9.97	.60	.80	49	322
2325	231	6.27	2.77	10.09	.58	.78	49	262
649	201	6.50	2.39	10.47	.70	.78	48	252
665	165	6.80	1.92	10.94	.86	.65	49	196
680	135	7.07	1.52	11.34	.74	.53	43	183
2291	125	7.16	1.39	11.47	.70	.48	− 20	187
690	92	7.43	1.02	11.84	.52	.44	+ 3	296
594	87	7.47	0.96	11.90	.52	.43	12	242
836	73	7.59	0.80	12.06	.56	.45	14	255
829	68	7.63	0.75	12.11	.55	.42	17	269
801	50	7.78	0.55	12.31	.61	.44	34	179
1434	− 20	8.03	0.22	12.64	.51	.48	+ 40	− 206
$l = 10°.9$								
625	− 313	5.87	4.30	7.62	.46	1.58	− 153	− 227
2293	282	6.08	3.66	8.26	.44	2.23	99	210
634	275	6.13	3.54	8.38	.68	1.72	104	261
2294	242	6.37	2.98	8.94	.60	1.01	94	223
642	237	6.40	2.92	9.00	.61	.88	104	259
650	199	6.67	2.38	9.54	.64	.78	56	301
2314	196	6.70	2.33	9.59	.68	.64	45	275
666	163	6.95	1.89	10.03	.84	.84	32	238
674	125	7.26	1.38	10.54	.81	.60	20	189
2304	114	7.34	1.25	10.67	.86	.52	22	242
691	89	7.52	0.97	10.95	.47	.93	6	206
769	84	7.56	0.91	11.01	.48	1.06	5	185
1445	− 53	7.80	0.56	11.36	.44	1.23	− 36	− 182
$l = 15°.9$								
643	− 234	6.55	3.13	7.75	1.06	.92	− 104	− 197
2326	224	6.62	2.94	7.94	.79	1.05	93	175
651	196	6.82	2.45	8.43	.60	.52	60	186
658	157	7.11	1.84	9.04	.64	.17	− 10	69
667	119	7.37	1.35	9.53	.56	.44	+ 2	190
814	110	7.44	1.22	9.66	.50	.55	− 3	207
2327	94	7.55	1.03	9.85	.42	.72	+ 2	147
692	85	7.61	0.93	9.95	.44	.71	− 3	185
774	69	7.72	0.75	10.13	.41	.93	0	150
775	49	7.86	0.52	10.36	.30	.69	+ 7	247
1446	− 35	7.96	0.36	10.52	.50	.64	+ 26	− 164

TABLE 5 (*continued*)

No. of measurement	f kc/s	R kpc	r_1 kpc	r_2 kpc	τ_1	τ_2	z_1 pc	z_2 pc
$l = 20°.9$								
2295	− 185	6.99	2.53	7.25	.54	.46	− 24	− 172
2316	158	7.18	2.02	7.76	.41	.33	33	186
2306	117	7.44	1.42	8.36	.43	.74	67	40
822	84	7.65	0.99	8.79	.48	.48	− 44	44
2305	− 37	7.96	0.41	9.37	.80	.70	+ 61	− 54
$l = 25°.9$								
2328	− 136	7.37	1.93	6.67	.56	.71	− 56	− 136
803	− 49	7.90	0.60	8.00	.40	.60	− 32	− 187
$l = 30°.9$								
834	− 108	7.57	1.78	5.56	.60	.74	− 87	− 76
2318	− 49	7.91	0.70	6.64	1.26	.46	− 94	− 108

solution must be carried out by successive approximations. The following method was used. First, approximate values of τ_1 and τ_2 are obtained by assuming values of b_1 and b_2. These four values are substituted in the equations (7) and the errors $\Delta I(b)$ determined. By differentiating (7) with respect to the four unknowns, these errors are expressed as linear combinations of the errors $\Delta\tau_1$, $\Delta\tau_2$, Δb_1 and Δb_2. The four linear equations obtained are solved for $\Delta\tau_1$, $\Delta\tau_2$, Δb_1 and Δb_2 and the originally assumed values are corrected for these errors. The same method may be carried from the second approximation to the third approximation, which always sufficed. In the actual reduction only three readings were made from the drift curves, one of them being the maximum intensity. This does not essentially alter the method described. The angles b_1 and b_2 were finally converted to linear heights above the galactic plane z_1 and z_2 with the known distances r_1 and r_2.

The results of this first separation of the contributions from the far and near points are given in Table 5. These results are not final, because no correction for the dispersion of random cloud velocities has yet been applied. The purpose of this first separation is to enable us to convert intensities into optical depths taking out the effect of the continuous radiation.

9. *Conversion of intensities into optical depths.*

The preceding results permit us to compute at each latitute b of a drift curve the optical depths $\tau_1(b)$ and $\tau_2(b)$. By substituting these into (5) we obtain the intensity $I_m(b)$. This "model" intensity corresponds to the hydrogen distribution tabulated in Tables 4 and 5. If the model is correct, this intensity $I_m(b)$ should be close to the measured intensity $I(b)$ of the drift curve. The agreement was satisfactory, in general.

We now reduce $I(b)$ to optical depth τ_u, neglecting the continuous radiation:

$$\tau_u = -\ln\left(1 - \frac{I(b)}{I_o}\right). \qquad (8)$$

The ratio $\gamma = \dfrac{\tau_1 + \tau_2}{\tau_u}$, which is the factor by which τ_u has to be multiplied in order to obtain the optical depth, corrected for continuous radiation, $\tau = \tau_1 + \tau_2$, is now known. Plots of γ against f, at each longitude and latitude where a line profile is available, were made by interpolation. Each line profile was then converted into τ_u by (8) and into total optical depth τ by multiplication with γ. The line profiles reduced to optical depth τ are shown in Figure 1.

10. *Correction for dispersion of cloud velocities.*

It is very difficult to obtain information on the distribution of peculiar velocities of hydrogen clouds in the inner parts of the Galactic System. KWEE, MULLER and WESTERHOUT [1]) state that the form of the profiles near maximum radial velocity suggests a gaussian distribution function more strongly than a distribution of the form $e^{-|v|/\eta}$, as found by BLAAUW [2]) from a study of interstellar lines. The unknown distribution of hydrogen along the observed part of the line of sight may, however, have distorted the form of the profiles near maximum radial velocity.

A discussion of the various methods that may be used to correct the line profiles for random cloud velocities is given by OLLONGREN and VAN DE HULST [3]). It was considered best to apply a second-difference correction

$$\tau' = \tau - \varepsilon\Delta^2\tau, \qquad (9)$$

similar to the correction applied for bandwidth; here ε is proportional to (dispersion)^2. The exact correction methods for gaussian and exponential distribution functions are compared with this approximate method (with $\varepsilon = 2$) in Figure 1 of the preceding paper [4]).

In the present investigation we have to assume that the dispersion of the cloud velocities changes with distance R from the galactic centre. In order to determine the coefficient ε as a function of R, recourse was made to a model of the distribution of mass in the Galactic System [5]); model 2 has been used. The

[1]) *Loc. cit.*
[2]) A. BLAAUW, *B.A.N.* **11**, 459 (No. 436), 1952.
[3]) *B.A.N.* **13**, 196 (No. 475, second paper), 1957.
[4]) G. WESTERHOUT, *B.A.N.* **13**, 201 (No. 475, third paper) 1957.
[5]) M. SCHMIDT, *B.A.N.* **13**, 15 (No. 468), 1956.

model gives $\frac{\partial Kz}{\partial z}$, the derivative of the force parallel to the galactic axis near the galactic plane. This quantity increases towards the galactic centre. In order to keep up a layer of constant thickness, as found in section 7, the velocity dispersion of the hydrogen in the z-direction should increase proportionally. This yields the velocity dispersion in the z-direction, σ_z, as a function of R. We need, however, the dispersion of velocities parallel to the galactic plane. The ratio of these dispersions is not known. Assuming that it does not depend on R, we find that

$$\varepsilon(R) = \text{constant} \,.\, \{\sigma_z(R)\}^2.$$

The constant is chosen in such a manner, that the minimum optical depth found between the arms after the correction (9), is zero or only slightly negative. This defines the maximum values of $\varepsilon(R)$. As the value found at $R = 8.2$ was $\varepsilon = 1.4$, somewhat smaller than the value used for the reduction of 21-cm measurements of the outer parts of the Galactic System, it was considered suitable to use these maximum values in the reduction. From the example given by WESTERHOUT it appears that the correction with $\varepsilon = 2$ gives the best approximation for a gaussian distribution with a dispersion $\sigma = 6$ km/sec. Corresponding values of σ for the other values of ε used are given as a function of R in Table 6 and Figure 5.

All line profiles were corrected for the dispersion of peculiar cloud velocities by means of these data. The corrected profiles τ' are shown in Figure 1.

Ideally we should find no contribution of optical depth in the corrected line profiles for radial velocities greater than the rotational velocity at each longitude.

TABLE 6

Values of the correction factor ε and the corresponding dispersion σ of the random cloud velocities.

R (kpc)	ε	σ (km/sec)
2	12.4	15.0
3	7.6	11.7
4	5.1	9.6
5	3.7	8.2
6	2.7	7.0
7	2.0	6.0
8.2	1.4	5.0

That this is not so will be due to small errors in the curve of the rotational velocities and to the rough method used to correct for the random cloud velocities. A correction will have to be applied to the optical depths at velocities close to the maximum velocity (section 13).

FIGURE 5

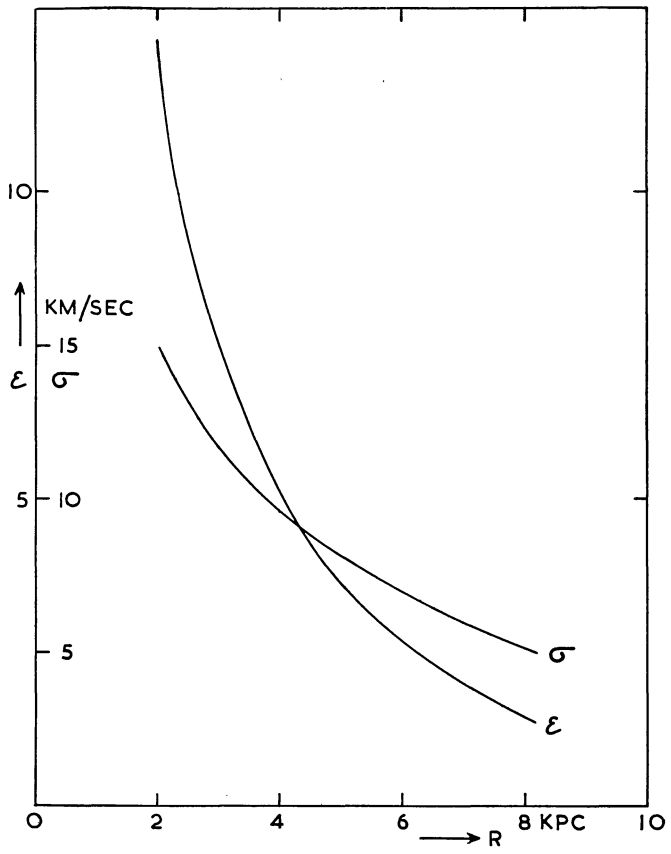

The correction factor ε and the corresponding dispersion σ of the random cloud velocities.

11. *z-distribution of hydrogen at different values of R.*

It is now possible to improve the results of section 7 and to derive a z-distribution of hydrogen, corrected for the effect of random cloud velocities. Use has been made of some of the best observed drift curves with a frequency somewhat below the maximum radial velocities. The factor $\frac{\tau'}{\tau}$, with which the optical depth τ at any latitude in a drift curve has to be multiplied to give the corrected optical depth τ', may be determined by interpolation from the line profiles at the same longitude l_0. This correction reduced the halfwidths of the drift curves by 2 to 7%. Accordingly, the thickness of the hydrogen layer now becomes 220 pc. The distribution used in the final separation is symmetric and identical to the negative half of the curve given in Figure 3 and Table 4, with $q = \frac{z - z_t}{110}$.

12. *Heights of the hydrogen layer above the galactic plane.*

The first separation (section 8) had shown that a denser net of points over the galactic plane was needed to give insight into the hydrogen distribution. The drift curves were observed at intervals of 5° in

longitude and 40 to 50 kc/s in frequency. The line profiles, however, are available at 2°.5 longitude intervals and may be read at 20 kc/s intervals. At this stage of the work it became clear that the spacing in latitude of the line profiles, which is only 2°, is still too large. If we want to determine optical depth and position of the far contributions, which may have an angular halfwidth less than 1°, it is necessary to have two line profiles which both contain a considerable intensity from that far contribution. It was impossible to obtain the additional profiles needed at $b = -0°.5$ and $-2°.5$ before the removal of the receiver from Kootwijk to Dwingeloo. However, these profiles could be constructed from the drift curves. For a correct interpolation in the 40 kc/s intervals, for which the drift curves are available, the line profiles at latitudes $+0°.5$, $-1°.5$ and $-3°.5$ were consulted. The resulting line profiles at latitudes $-0°.5$ and $-2°.5$ were further reduced in the same way as the other profiles.

With these supplementary profiles the material thus consists of optical depths at each 5° interval of longitude and each 20 kc/s interval of frequency, at latitudes $+0°.5$, $-0°.5$, $-1°.5$, $-2°.5$ and $-3°.5$.

A second separation of contributions in optical depths, similar to the separation described in section 8, was now carried out. This separation was based on the equation

$$\tau'(b) = \tau_1' a_1(b, b_1) + \tau_2' a_2(b, b_2), \qquad (10)$$

which is much simpler than equation (7). Again, the values of τ_1, τ_2, b_1 and b_2 were obtained by successive approximations. The angles b_1 and b_2 were converted to linear heights, z_1 and z_2, above the galactic plane. They are given in Table 9.

This separation still does not represent the final result, because accidental errors in z_2 may introduce systematic errors in τ_2'. If we consider a latitude distribution $\tau(b)$ at a frequency for which the ratio of r_1 and r_2 is great and at which τ_2' is small, then the second contribution forms only a very low and narrow hump on top of the first contribution. Errors in the measurements, which are much enlarged by the correction for peculiar cloud velocities, may make the optical depth at one of the latitudes somewhat too large. It is then quite probable that a spurious hump occurs, which in the separation is attributed to the second, narrow contribution. Thus irregular values of z_2 and too large values of τ_2' may be introduced.

To avoid these systematic errors the z-values were smoothed. This smoothing process was carried out in graphs of z against L in intervals of $\frac{1}{2}$ kpc in R, where L is the galactocentric longitude, which increases in the same sense as the galactic longitude l. The direction towards the sun is $L = 0°$. Smoothing over L seems preferable to smoothing over r because

FIGURE 6

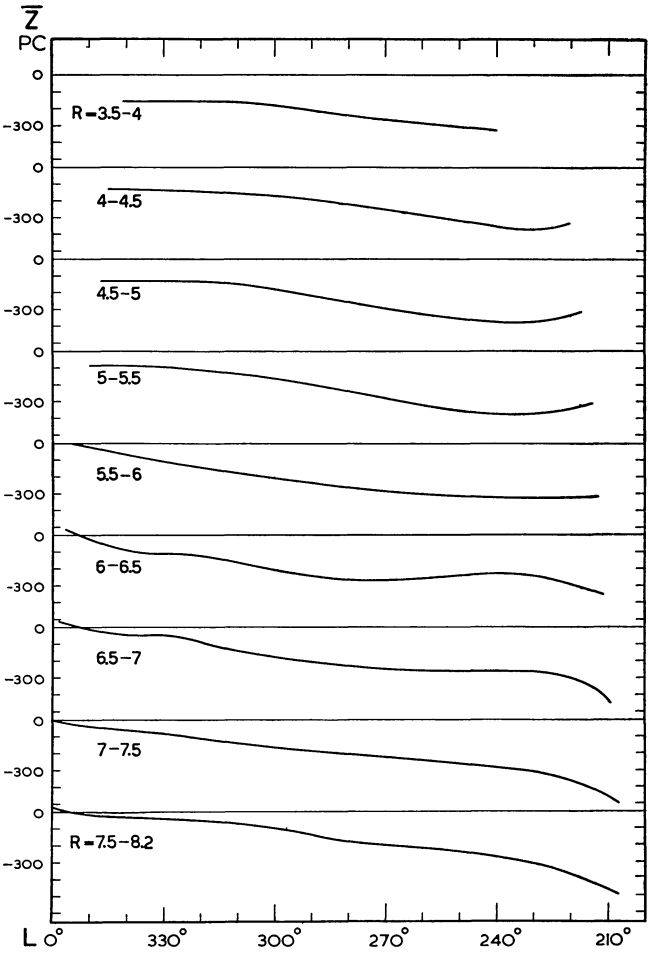

Smoothed curves of height $\bar{z}$ above the galactic plane, as a function of galactocentric longitude L, in intervals of 0.5 kpc in R. (Sun has $L = 0°$).

separate spiral arms may well have different heights, while in one spiral arm only gradual changes of height may be expected. The smoothed curves $\bar{z}(L)$ are shown in Figure 6, while the corresponding curves $\bar{z}(r)$ are given in Figure 7 and in Table 9.

WESTERHOUT [1]) has used the values of $\bar{z}$ from Figure 7, together with values of z for the region $R > 8.2$ kpc, to determine the position of a mean galactic plane. The position of this plane is indicated in Figure 7 by dashed lines. The average deviation from the mean plane of the hydrogen in the region discussed here is ± 32 pc.

13. *Final separation and calculation of hydrogen densities.*

The separation described in the previous section may now be repeated, taking the values of $\bar{z}_1$ and $\bar{z}_2$ from Table 9. Whenever one of the τ-values became negative, the value was taken to be zero and the

[1]) L.c., section 16, p. 217 of this Bulletin.

FIGURE 7

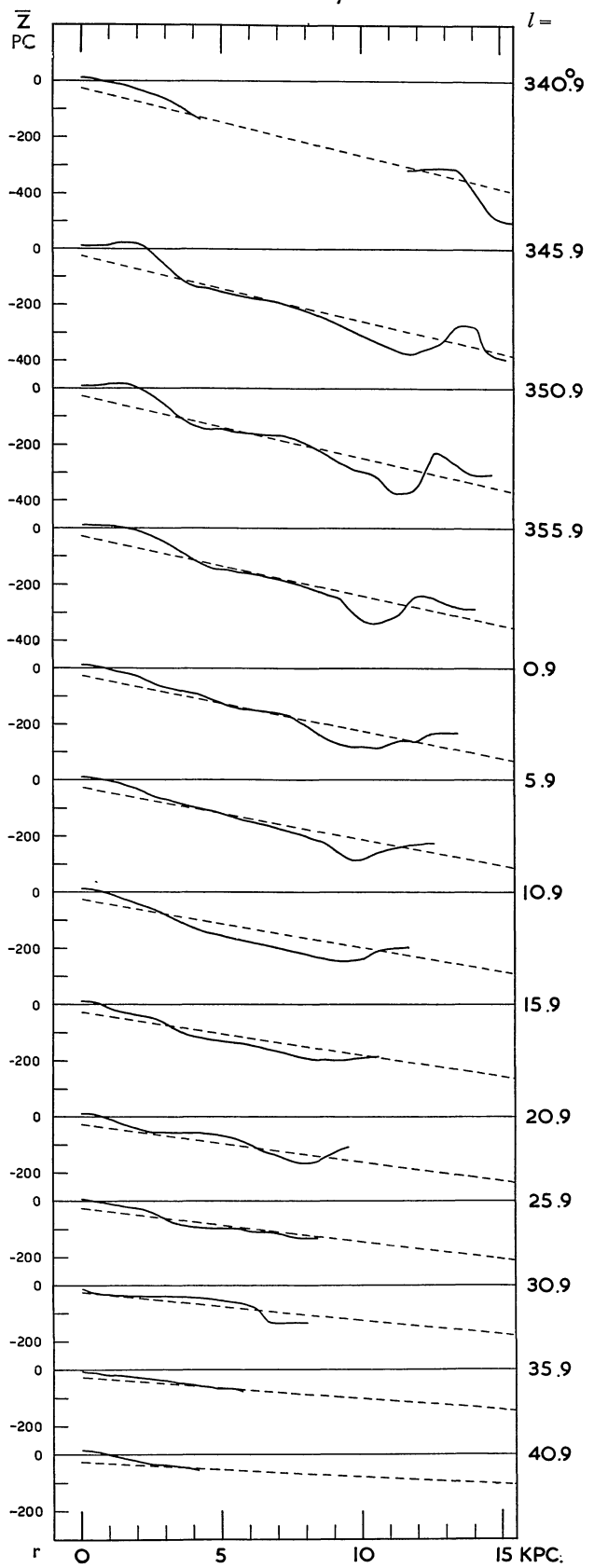

Smoothed curves of height $\bar{z}$ above the galactic plane, as a function of distance to the sun r. The dashed lines give the position of a mean galactic plane with the pole $l = 322°$, $b = 88°.56$*.

*) Third paper of this series, section 16, p. 217.

separation repeated. The resulting values of τ_1' and τ_2' are given in Table 9.

The relation between the optical depth τ' and the hydrogen density n_H is given in atoms per cm³ by [1])

$$n_H = 0.0744\,\tau'\,dV_g/dr \qquad (11)$$

if $T = 125°$K.

Here $\frac{dV_g}{dr}$ is expressed in km/sec. kpc and is computed from

$$dV_g/dr = \frac{R_m}{R}\sqrt{R^2 - R_m^2}\,\frac{\partial\omega}{\partial R}\,. \qquad (12)$$

The conversion factor n_H/τ' is listed in Table 9 together with the resulting hydrogen densities n_1 and n_2.

The densities were projected on the galactic plane and curves of equal density $n_H = 0.2$, 0.6, 1.0 and 1.6 atoms per cm³ were drawn. The resulting map is shown in Plate B (opposite p. 247). The isodensity contours near the circle $R = 8.2$ kpc are necessarily somewhat arbitrary. No separation has been carried out if the ratio r_2/r_1 was smaller than 1.8. The region to which this applies is indicated by two thick circles in the figure. In this region the optical depths of the two contributions were taken equal for lack of better information.

For the region between $l = 40°.9$ and $57°.5$, $R < 8.2$ kpc, which was not studied in this investigation, WESTERHOUT, after a careful study of plots of optical depth against latitude and radial velocity, concluded that most of the hydrogen is situated in the far points; he has drawn the isodensity contours accordingly.

We still have to account for the optical depths found at velocities higher than the rotational velocities. The relation to the hydrogen density is obtained by integrating (11)

$$\int n_H\,dr = \bar{n}_H\,.\,\Delta r = .0744\int_{V_g > V_{max}} \tau'(V_g)\,dV_g\,. \qquad (12)$$

The left-hand side represents the number of hydrogen atoms per cm³ along the line of sight to be added to the number already obtained. It is listed in Table 7 in the unit kpc/cm³. These additional hydrogen atoms have been distributed as well as possible over 2 kpc of the line of sight, situated symmetrically with respect to the midpoint of the line of sight. In some directions the hydrogen densities are considerably changed by this addition. These changes have been taken into account in drawing the isodensity contours in Plate B.

[1]) *B.A.N.* **12**, 117 (No. 452), 1954, eqs. (12) and (18).

TABLE 7

Number of hydrogen atoms along the line of sight with velocities higher than the rotational velocities.

l	$\bar{n}_H.\Delta r$ kpc/cm³	l	$\bar{n}_H.\Delta r$ kpc/cm³
°		°	
345.9	+.19	15.9	+.35
348.4	−.05	18.4	+.30
350.9	−.04	20.9	+.55
353.4	+.01	23.4	+.14
355.9	−.01	25.9	+.18
358.4	+.29	28.4	+.13
0.9	+.31	30.9	+.11
3.4	+.15	33.4	+.04
5.9	+.27	35.9	+.04
8.4	+.01	38.4	+.03
10.9	−.12	40.9	+.05
13.4	+.01		

14. *Interpretation and discussion of the results.*

The final results consist of:

a. the maximum hydrogen density, Table 9, Plate B (opposite p. 247).

b. the height $\bar{z}$ of the maximum hydrogen density, Table 9, Figures 6 and 7.

c. the relative distribution of hydrogen density in the z-direction, Table 4, Figure 3, where $q = (z - \bar{z})/110$ pc.

In examining these results it should be noted that the data for each longitude have been treated entirely independently, except for the smoothing of $\bar{z}$ (section 12), which cannot have affected the densities.

Perusal of Plate B shows the following features. The *Orion arm* may be followed from $l = 220°$ down to $l = 341°$, which is the lower longitude limit of the present investigation. Between $l = 220°$ and $l = 50°$ it lies mainly outside the circle $R = 8.2$ kpc. There seems to be a break in the arm between $l = 25°$ and $l = 35°$, where it splits up into two separate parts, one inside and one outside the circle $R = 8.2$ kpc. The next arm, seen tangentially at $l = 18°$, extends to the region in Sagittarius where MORGAN, CODE

TABLE 8

Average densities in the near and the far points.

	$\bar{n}_1$	$\bar{n}_2$
$6 < R < 8.2$	.84 cm^{-3}	.86 cm^{-3}
$R < 6$	.40	.68

TABLE 9

Final results of the separations; the distance from the sun is r, the height above the galactic plane of the points of maximum density in the z-direction is $\bar{z}$, and the value of this density is n.

f kc/s	R kpc	r_1 kpc	r_2 kpc	z_1 pc	z_2 pc	τ_1'	τ_2'	n_H/τ'	n_1 cm^{-3}	n_2 cm^{-3}	$\bar{z}_1$ pc	$\bar{z}_2$ pc
$l = 340°.9$												
20	7.75	0.47	15.49		− 482	1.10	.95	.66	.72	.63	+ 9	− 505
40	7.30	0.93	15.03	0	515	.94	1.86	.67	.63	1.25	0	493
60	6.84	1.41	14.55	− 42	495	1.32	1.98	.68	.90	1.36	− 9	460
80	6.40	1.87	14.09	15	385	1.96	.01	.71	1.39	.01	22	396
100	5.98	2.31	13.65			1.45	.00	.74	1.08	.00	36	329
120	5.61	2.70	13.26	66	282	.63	2.45	.80	.50	1.95	52	312
140	5.26	3.08	12.88	74	309	.49	3.23	.89	.43	2.87	66	309
160	4.93	3.43	12.53	85	288	.86	.95	1.00	.86	.95	86	309
180	4.67	3.71	12.25	85	301	.47	1.86	1.08	.51	2.01	102	311
200	4.42	3.99	11.97	− 140	− 411	.70	.00	1.17	.82	.00	121	316
220	4.17	4.27	11.69			.18	1.02	1.25	.22	1.28	− 139	− 319
$l = 343°.4$												
20	7.82	0.40	15.38			1.19	.36	.77	.91	.28	+ 10	− 451
40	7.44	0.80	14.98			.75	.55	.78	.58	.43	6	439
60	7.06	1.20	14.58			.83	.91	.79	.65	.72	+ 2	407
80	6.69	1.59	14.19			1.29	.65	.81	1.04	.52	− 1	339
100	6.31	1.99	13.79			1.93	.00	.82	1.59	.00	7	301
120	5.96	2.37	13.41			.90	1.39	.86	.78	1.20	19	297
140	5.64	2.72	13.06			.90	2.09	.92	.83	1.92	35	311
160	5.34	3.05	12.73			.39	1.30	1.00	.39	1.29	62	326
180	5.05	3.37	12.41			.27	1.51	1.09	.29	1.65	84	333
200	4.80	3.65	12.13			.00	.44	1.19	.00	.52	104	340
220	4.59	3.89	11.89			.00	1.77	1.26	.00	2.23	124	346
240	4.38	4.13	11.65			.56	.29	1.33	.74	.39	135	346
260	4.17	4.38	11.40			.00	.79	1.40	.00	1.11	− 146	− 346

TABLE 9 (*continued*)

f kc/s	R kpc	r_1 kpc	r_2 kpc	z_1 pc	z_2 pc	τ_1'	τ_2'	n_H/τ'	n_1 cm^{-3}	n_2 cm^{-3}	$\bar{z}_1$ pc	$\bar{z}_2$ pc
$l = 345°.9$												
20	7.87	0.35	15.21			1.13	.00	.87	.98	.00	+ 11	− 396
40	7.54	0.70	14.86	− 92	− 329	.66	1.02	.88	.57	1.24	11	385
60	7.22	1.04	14.52	+ 15	514	.79	.35	.89	.71	.41	13	365
80	6.87	1.42	14.14	43	304	1.15	4.39	.90	1.04	3.96	20	282
100	6.53	1.79	13.77	+ 35	262	2.15	3.26	.91	1.97	2.98	22	275
120	6.23	2.11	13.45	− 24	373	1.34	1.48	.94	1.25	1.39	+ 14	280
140	5.93	2.45	13.11	+ 15	337	1.20	.97	.97	1.16	.94	− 6	314
160	5.66	2.75	12.81			.11	1.77	1.02	.11	1.81	38	342
180	5.40	3.04	12.52			.30	.00	1.09	.33	.00	66	355
200	5.14	3.34	12.22			.47	.66	1.18	.55	.78	88	364
220	4.92	3.60	11.96	− 123	484	.29	1.49	1.26	.37	1.88	110	374
240	4.72	3.83	11.73		387	.01	1.93	1.33	.01	2.57	125	377
260	4.53	4.06	11.50			.00	1.50	1.39	.00	2.08	133	372
280	4.35	4.29	11.27	− 158	386	.00	1.30	1.45	.00	1.88	138	363
300	4.17	4.51	11.05		− 390	.00	1.29	1.51	.00	1.95	140	356
320	4.01	4.72	10.84			.37	.12	1.54	.57	.18	144	346
340	3.86	4.92	10.64			.20	.41	1.59	.32	.65	152	337
360	3.72	5.11	10.45			.04	.07	1.64	.07	.11	155	328
380	3.58	5.31	10.25			.01	.02	1.69	.02	.00	158	320
400	3.45	5.50	10.06			.02	.00	1.71	.03	.00	164	310
420	3.34	5.67	9.89			.03	.14	1.72	.12	.12	166	304
440	3.23	5.85	9.71			.12	.12	1.71	.21	.21	172	296
460	3.13	6.02	9.54			.08	.08	1.69	.14	.14	173	289
480	3.03	6.21	9.35			.08	.08	1.62	.13	.13	178	277
500	2.93	6.41	9.15			.08	.08	1.55	.12	.12	179	268
520	2.84	6.62	8.94			.00	.00	1.42	.00	.00	184	261
540	2.75	6.86	8.70			.14	.14	1.22	.17	.17	187	248
560	2.66	7.17	8.39			.15	.15	.87	.13	.13	− 194	− 233
$l = 348°.4$												
20	7.90	0.32	15.00			.94	.08	.96	.91	.08	+ 11	− 308
40	7.62	0.63	14.69			.85	.00	.97	.82	.00	11	308
60	7.33	0.94	14.38			.22	2.15	.98	.22	2.10	13	304
80	7.03	1.27	14.05			.91	3.35	.99	.90	3.30	18	292
100	6.73	1.60	13.72			1.18	3.21	1.00	1.18	3.21	20	277
120	6.44	1.92	13.40			1.04	1.11	1.01	1.05	1.12	+ 13	270
140	6.17	2.23	13.09			.68	1.13	1.03	.70	1.16	− 2	277
160	5.91	2.53	12.79			.66	.00	1.06	.70	.00	28	288
180	5.67	2.81	12.51			.13	.81	1.10	.14	.89	50	318
200	5.44	3.08	12.24			.20	1.19	1.16	.23	1.38	68	350
220	5.21	3.35	11.97			.39	.58	1.24	.48	.72	90	372
240	5.00	3.61	11.71			.27	.44	1.31	.35	.58	108	376
260	4.81	3.85	11.47			.08	.82	1.38	.11	1.13	121	374
280	4.65	4.05	11.27			.26	.43	1.42	.37	.61	132	367
300	4.49	4.26	11.06			.01	.71	1.47	.01	1.04	136	356
320	4.33	4.47	10.85			.00	.87	1.50	.00	1.30	143	342
340	4.17	4.69	10.63			.18	.46	1.54	.28	.71	147	328
360	4.02	4.91	10.41			.00	.84	1.56	.00	1.31	150	318
380	3.89	5.10	10.22			.31	.07	1.58	.49	.11	151	310
400	3.76	5.30	10.02			.42	.27	1.59	.67	.43	156	301
420	3.64	5.50	9.82			.11	.11	1.59	.17	.17	161	294
440	3.53	5.69	9.63			.35	.35	1.57	.55	.55	164	286
460	3.42	5.90	9.42			.20	.20	1.54	.31	.31	165	278
480	3.32	6.10	9.22			.01	.01	1.46	.01	.01	170	266
500	3.22	6.32	9.00			.00	.00	1.36	.00	.00	172	253
520	3.13	6.56	8.76			.08	.08	1.20	.10	.10	174	240
540	3.04	6.85	8.47			.33	.33	.94	.31	.31	176	220
560	2.94	7.42	7.90			.71	.71	.30	.22	.22	− 187	− 198
$l = 350°.9$												
20	7.94	.28	14.76			.98	.00	1.06	1.04	.00	+ 11	− 308
40	7.68	.57	14.47			.60	.76	1.06	.64	.81	+ 11	− 308

TABLE 9 (*continued*)

f kc/s	R kpc	r_1 kpc	r_2 kpc	z_1 pc	z_2 pc	τ_1'	τ_2'	n_H/τ'	n_1 cm^{-3}	n_2 cm^{-3}	$\bar{z}_1$ pc	$\bar{z}_2$ pc
$l = 350°.9$												
60	7.41	.87	14.17	− 150	− 268	.60	1.33	1.06	.64	1.41	+ 13	− 309
80	7.16	1.15	13.89	+ 99	315	.69	1.43	1.06	.73	1.52	16	301
100	6.88	1.46	13.58			.80	.97	1.07	.86	1.04	19	280
120	6.61	1.77	13.27	58	264	.51	1.57	1.08	.55	1.70	+ 11	258
140	6.37	2.05	12.99	+ 41	211	.48	1.28	1.10	.53	1.41	0	242
160	6.12	2.34	12.70			.62	.36	1.11	.69	.40	− 16	233
180	5.88	2.63	12.41		250:	.23	1.82	1.14	.26	2.07	33	280
200	5.67	2.88	12.16			.27	.91	1.18	.32	1.07	50	336
220	5.46	3.14	11.90	− 47	431	.19	2.00	1.22	.23	2.44	72	368
240	5.26	3.39	11.65	48	442	.21	1.92	1.28	.27	2.46	91	376
260	5.06	3.65	11.39	244	404	.07	1.69	1.35	.09	2.28	110	376
280	4.88	3.89	11.15	156	397	.32	.87	1.40	.45	1.22	125	372
300	4.73	4.09	10.95	227	359	.21	1.46	1.44	.30	2.10	133	358
320	4.58	4.30	10.74			.22	.00	1.48	.33	.00	142	338
340	4.44	4.51	10.53			.14	.75	1.49	.21	1.12	144	320
360	4.29	4.73	10.31		342:	.00	1.65	1.50	.00	2.48	144	308
380	4.15	4.95	10.09	198	213	.29	.30	1.50	.44	.45	143	299
400	4.03	5.15	9.89	147	328	.35	.27	1.49	.52	.40	148	292
420	3.90	5.38	9.66	− 154	324	.24	.24	1.46	.35	.35	154	284
440	3.79	5.59	9.45			.45	.45	1.42	.64	.64	156	276
460	3.68	5.81	9.23		− 283	.75	.75	1.37	1.03	1.03	157	267
480	3.57	6.06	8.98			.61	.61	1.26	.77	.77	163	254
500	3.47	6.33	8.71			.50	.50	1.11	.56	.56	165	236
520	3.39	6.59	8.45			.52	.52	.91	.47	.47	165	220
540	3.29	7.08	7.96			.32	.32	.47	.15	.15	− 166	− 191
$l = 353°.4$												
20	7.96	.27	14.49			1.01	.01	1.13	1.25	.01	+ 11	− 297
40	7.72	.54	14.22			.44	.47	1.14	.50	.54	11	297
60	7.48	.81	13.95			.31	.77	1.13	.35	.87	11	297
80	7.25	1.08	13.68			.78	1.28	1.14	.89	1.46	13	290
100	7.00	1.36	13.40			.52	2.07	1.14	.59	2.36	12	275
120	6.75	1.66	13.10			.31	2.55	1.15	.36	2.93	+ 6	260
140	6.52	1.93	12.83			.09	1.69	1.15	.10	1.94	0	244
160	6.29	2.21	12.55			.74	.00	1.16	.86	.00	− 14	238
180	6.07	2.48	12.28			.43	.54	1.18	.51	.64	28	262
200	5.86	2.74	12.02			1.03	.00	1.20	1.24	.00	42	296
220	5.67	2.98	11.78			.70	.15	1.23	.86	.18	59	329
240	5.48	3.23	11.53			.29	.53	1.27	.37	.67	75	344
260	5.29	3.49	11.27			.32	.55	1.30	.42	.72	91	350
280	5.11	3.73	11.03			.54	.78	1.35	.73	1.05	107	352
300	4.95	3.96	10.80			.26	1.38	1.40	.36	1.93	117	350
320	4.79	4.20	10.56			.26	.00	1.42	.37	.00	128	340
340	4.66	4.40	10.36			.47	.45	1.43	.67	.64	134	326
360	4.53	4.60	10.16			.00	.36	1.44	.00	.52	139	314
380	4.40	4.82	9.94			.09	.22	1.43	.13	.10	142	298
400	4.27	5.05	9.71			.00	.32	1.40	.00	.45	145	290
420	4.14	5.30	9.46			.42	.42	1.36	.57	.57	152	266
440	4.02	5.55	9.21			.65	.65	1.27	.83	.83	155	257
460	3.91	5.81	8.95			.42	.42	1.17	.49	.49	156	246
480	3.81	6.08	8.68			.92	.92	1.04	.96	.96	163	233
500	3.71	6.41	8.35			.57	.57	.83	.47	.47	172	213
520	3.60	7.00	7.76			.39	.39	.35	.14	.14	− 176	− 187
$l = 355°.9$												
20	7.98	.25	14.17			.00	.73	1.21	.00	.88	+ 11	− 286
40	7.76	.50	13.92	0	− 187	.38	.48	1.20	.46	.58	11	286
60	7.54	.77	13.65			.46	1.03	1.20	.55	1.24	10	286
80	7.33	1.00	13.42	− 86	263	.73	.64	1.20	.88	.77	10	280
100	7.11	1.27	13.15			.76	2.10	1.20	.91	2.52	+ 6	271
120	6.88	1.54	12.88			.33	2.27	1.20	.40	2.72	0	261
140	6.65	1.82	12.60	− 14	− 264	.16	1.95	1.21	.19	2.36	0	− 248

TABLE 9 (*continued*)

f kc/s	R kpc	r_1 kpc	r_2 kpc	z_1 pc	z_2 pc	τ_1'	τ_2'	n_H/τ'	n_1 cm^{-3}	n_2 cm^{-3}	$\bar{z}_1$ pc	$\bar{z}_2$ pc
$l = 355°.9$												
160	6.44	2.09	12.33	+ 26	− 243	.19	1.13	1.20	.23	1.36	− 12	− 242
180	6.24	2.34	12.08	+ 13	222	.47	.37	1.21	.57	.45	22	242
200	6.03	2.61	11.81	− 30	340	.78	.19	1.21	.94	.23	35	256
220	5.85	2.85	11.57	59	353	.68	.00	1.24	.84	.00	46	289
240	5.67	3.09	11.33			.19	.32	1.25	.24	.40	58	312
260	5.49	3.35	11.07	119	320	.20	.25	1.27	.25	.32	73	324
280	5.32	3.59	10.83	− 57		.38	.00	1.30	.49	.00	88	333
300	5.15	3.85	10.57	+ 24	− 235	.64	.00	1.33	.85	.00	101	341
320	5.00	4.08	10.34	− 117:		.73	.00	1.35	.99	.00	113	342
340	4.85	4.33	10.09			.60	.72	1.35	.81	.97	124	332
360	4.72	4.55	9.87	− 169		.57	.55	1.35	.77	.74	133	319
380	4.60	4.77	9.65			.37	.73	1.32	.49	.96	141	297
400	4.48	5.01	9.41			.59	.41	1.28	.76	.52	143	269
420	4.36	5.26	9.16			.53	.53	1.20	.64	.64	148	249
440	4.23	5.57	8.85			.77	.77	1.09	.84	.84	154	240
460	4.12	5.88	8.54			.62	.62	.95	.59	.59	156	227
480	4.02	6.24	8.18			.39	.39	.73	.28	.28	164	213
500	3.91	6.93	7.49			.27	.27	.23	.06	.06	− 179	− 191
$l = 358°.4$												
20	8.00	.24	13.84			.62	.89	1.26	.78	1.12	+ 11	− 258
40	7.79	.49	13.59			.81	.00	1.26	1.02	.00	9	258
60	7.59	.72	13.36			1.11	.00	1.26	1.40	.00	7	258
80	7.39	.97	13.11			.40	1.46	1.25	.50	1.82	+ 4	256
100	7.19	1.21	12.87			.47	2.95	1.25	.59	3.69	0	253
120	6.98	1.47	12.61			.49	3.21	1.25	.61	4.01	− 6	254
140	6.77	1.74	12.34			.54	.90	1.24	.67	1.12	9	255
160	6.56	2.01	12.07			.30	.00	1.24	.37	.00	20	253
180	6.37	2.26	11.82			.55	.20	1.24	.68	.25	29	253
200	6.18	2.52	11.56			.38	1.51	1.23	.47	1.86	42	263
220	6.00	2.76	11.32			.62	.55	1.23	.76	.68	53	282
240	5.82	3.02	11.06			.28	.57	1.24	.35	.71	62	298
260	5.66	3.26	10.82			.54	.12	1.24	.67	.15	73	306
280	5.50	3.50	10.58			.27	.00	1.25	.34	.00	84	308
300	5.34	3.75	10.33			.65	.00	1.27	.83	.00	92	311
320	5.18	4.02	10.06			.78	.09	1.27	.99	.11	101	310
340	5.03	4.29	9.79			.40	.81	1.26	.50	1.02	112	304
360	4.90	4.53	9.55			.33	.97	1.24	.41	1.20	121	293
380	4.77	4.80	9.28			1.22	.10	1.19	1.45	.12	133	276
400	4.66	5.04	9.04			.38	.38	1.13	.43	.43	138	255
420	4.55	5.31	8.77			1.00	1.00	1.04	1.04	1.04	143	235
440	4.44	5.63	8.45			.70	.70	.90	.63	.63	148	214
460	4.32	6.07	8.01			.90	.90	.66	.60	.60	− 160	− 192
$l = 0°.9$												
20	8.01	.23	13.47	+ 4	− 130	.61	.35	1.32	.81	.46	+ 10	− 231
40	7.82	.46	13.24			.91	.00	1.31	1.19	.00	8	231
60	7.63	.70	13.00			1.30	.18	1.30	1.69	.23	+ 2	231
80	7.44	.93	12.77	− 32	235	.60	1.78	1.30	.78	2.31	− 1	232
100	7.26	1.16	12.54			.28	2.59	1.29	.36	3.34	7	236
120	7.07	1.41	12.29			.51	1.31	1.28	.65	1.68	11	248
140	6.86	1.68	12.02			.49	1.09	1.27	.62	1.38	19	262
160	6.67	1.94	11.76	26	218	.18	1.01	1.26	.23	1.27	26	264
180	6.49	2.18	11.52			.55	.00	1.25	.69	.00	35	264
200	6.31	2.44	11.26	42		.87	.00	1.24	1.08	.00	47	270
220	6.13	2.70	11.00	64	250	.97	.19	1.23	1.19	.23	60	275
240	5.96	2.95	10.75	64	250	.96	.52	1.22	1.17	.63	66	284
260	5.80	3.20	10.50	158	177	.54	1.19	1.21	.65	1.44	73	286
280	5.65	3.45	10.25	99	374	.40	.00	1.20	.48	.00	79	283
300	5.50	3.70	10.00			.26	.00	1.19	.31	.00	84	282
320	5.35	3.97	9.73			.16	.36	1.18	.19	.42	88	278
340	5.20	4.26	9.44	90	58	.39	.24	1.15	.45	.28	99	275
360	5.06	4.56	9.14	− 70	− 92	.60	.09	1.10	.66	.10	− 110	− 267

TABLE 9 (*continued*)

f kc/s	R kpc	r_1 kpc	r_2 kpc	z_1 pc	z_2 pc	τ_1'	τ_2'	n_H/τ'	n_1 cm^{-3}	n_2 cm^{-3}	$\bar{z}_1$ pc	$\bar{z}_2$ pc
$l = 0°.9$												
380	4.93	4.86	8.84	− 88	− 172	.24	.84	1.04	.25	.87	− 124	− 255
400	4.81	5.18	8.52	− 150	− 90	.56	.56	.93	.52	.52	132	240
420	4.71	5.49	8.21			.80	.80	.80	.64	.64	139	221
440	4.60	5.94	7.76			.52	.52	.57	.30	.30	− 143	− 189
$l = 3°.4$												
20	8.02	.22	13.06			.68	.34	1.36	.92	.46	+ 10	− 229
40	7.85	.44	12.84			1.13	.00	1.35	1.53	.00	7	229
60	7.67	.67	12.61			.84	.86	1.34	1.13	1.15	+ 2	229
80	7.49	.90	12.38			.58	.89	1.33	.77	1.18	0	231
100	7.31	1.14	12.14			.44	.14	1.32	.58	.18	− 4	233
120	7.14	1.36	11.92			.81	.00	1.31	1.06	.00	11	243
140	6.95	1.62	11.66			1.23	.00	1.30	1.60	.00	20	252
160	6.76	1.89	11.39			.96	.59	1.28	1.23	.76	26	257
180	6.59	2.14	11.14			.66	.84	1.26	.83	1.06	35	261
200	6.42	2.39	10.89			.46	1.38	1.24	.57	1.71	48	268
220	6.25	2.65	10.63			.58	.00	1.22	.71	.00	60	274
240	6.09	2.90	10.38			.91	.99	1.20	1.09	1.19	67	284
260	5.93	3.17	10.11			1.27	.72	1.17	1.49	.84	75	286
280	5.78	3.43	9.85			.38	1.20	1.15	.44	1.38	81	277
300	5.64	3.69	9.59			.19	.50	1.12	.21	.56	86	268
320	5.50	3.97	9.31			.00	.21	1.08	.00	.23	92	256
340	5.36	4.27	9.01			.15	.00	1.03	.15	.00	101	246
360	5.22	4.61	8.67			.60	.00	.95	.57	.00	111	235
380	5.08	5.01	8.27			.91	.91	.83	.76	.76	125	222
400	4.96	5.43	7.85			.40	.40	.66	.26	.26	144	198
420	4.85	6.02	7.26			.48	.48	.36	.17	.17	− 154	− 192
$l = 5°.9$												
20	8.03	.22	12.64	+ 51	− 223	.77	1.74	1.39	1.07	2.42	+ 10	− 226
40	7.86	.44	12.42	− 42		.99	.17	1.38	1.37	.23	7	226
60	7.70	.65	12.21	+ 68	264	.73	.69	1.37	1.00	.95	2	228
80	7.53	.88	11.98			.59	.34	1.35	.80	.46	+ 1	230
100	7.36	1.11	11.75	+ 24	231	.56	.37	1.35	.76	.50	− 3	231
120	7.20	1.34	11.52	− 2	463	.84	.15	1.32	1.11	.20	11	239
140	7.02	1.60	11.26			1.29	.00	1.28	1.65	.00	20	242
160	6.85	1.85	11.01	+ 3	242	1.27	1.01	1.28	1.63	1.29	25	250
180	6.68	2.10	10.76	− 1	214	.84	1.27	1.26	1.06	1.60	36	257
200	6.51	2.37	10.49	22	245	.59	1.24	1.22	.72	1.51	50	266
220	6.36	2.62	10.24	143	197	.20	.90	1.20	.24	1.08	60	273
240	6.20	2.89	9.97	57	285	.48	.79	1.16	.56	.92	68	283
260	6.04	3.18	9.68	78	350	.56	1.80	1.12	.63	2.02	76	286
280	5.89	3.47	9.39	59	348	.42	1.74	1.08	.45	1.88	82	273
300	5.75	3.76	9.10	57	252	.47	1.42	1.02	.48	1.45	88	255
320	5.62	4.05	8.81			.51	.42	.96	.49	.40	97	234
340	5.49	4.37	8.49	88	243	.76	.50	.89	.68	.44	102	218
360	5.35	4.78	8.08	− 142	144	.66	.66	.76	.50	.50	112	205
380	5.22	5.27	7.59		− 188	.77	.77	.58	.44	.44	128	189
400	5.09	6.43	6.43			.76	.76	.00	.00	.00	− 156	− 156
$l = 8°.4$												
20	8.04	.22	12.18			.95	.16	1.41	1.34	.23	+ 11	− 213
40	7.88	.43	11.97			.99	.89	1.39	1.38	1.24	8	213
60	7.72	.65	11.75			.44	1.10	1.38	.61	1.52	+ 2	215
80	7.56	.88	11.52			.29	1.83	1.36	.39	2.49	0	218
100	7.41	1.09	11.31			.44	.40	1.35	.59	.54	− 8	221
120	7.25	1.33	11.07			.69	.41	1.32	.91	.54	15	226
140	7.09	1.57	10.83			1.22	.92	1.29	1.57	1.19	22	234
160	6.92	1.84	10.56			1.64	.45	1.27	2.08	.57	29	246
180	6.75	2.11	10.29			1.73	.00	1.23	2.13	.00	38	252
200	6.59	2.38	10.02			.89	.65	1.19	1.06	.77	− 51	− 256

TABLE 9 (*continued*)

f kc/s	R kpc	r_1 kpc	r_2 kpc	z_1 pc	z_2 pc	τ_1'	τ_2'	n_H/τ'	n_1 cm^{-3}	n_2 cm^{-3}	$\bar{z}_1$ pc	$\bar{z}_2$ pc
$l = 8°.4$												
220	6.44	2.65	9.75			.42	.00	1.15	.48	.00	− 64	− 260
240	6.30	2.91	9.49			.45	.47	1.11	.50	.52	75	264
260	6.15	3.20	9.20			.83	.07	1.05	.87	.07	86	261
280	6.00	3.52	8.88			.23	2.75	.98	.23	2.71	97	251
300	5.86	3.85	8.55			.99	3.17	.91	.90	2.88	108	238
320	5.73	4.20	8.20			.73	2.38	.81	.59	1.94	119	222
340	5.61	4.58	7.82			1.13	1.13	.69	.78	.78	128	209
360	5.48	5.11	7.29			.12	.12	.50	.06	.06	− 143	− 183
$l = 10°.9$												
20	8.05	.21	11.71			.88	.47	1.42	1.25	.67	+ 11	− 200
40	7.90	.42	11.50	+ 91	− 218	.51	2.22	1.40	.71	3.11	9	200
60	7.75	.64	11.28	− 9	196	.20	2.19	1.38	.28	3.02	+ 2	201
80	7.59	.87	11.05	73	202	.23	1.88	1.35	.31	2.54	− 1	203
100	7.44	1.10	10.82	7	220	.57	1.44	1.33	.76	1.92	12	209
120	7.29	1.33	10.59	165	46	.71	.28	1.30	.92	.36	19	213
140	7.14	1.57	10.35			1.04	.00	1.27	1.32	.00	24	224
160	6.98	1.83	10.09	8	202	.76	1.95	1.24	.94	2.42	33	240
180	6.82	2.11	9.81	66	267	.97	1.59	1.20	1.16	1.91	41	244
200	6.66	2.40	9.52	42	452	1.08	.00	1.15	1.24	.00	52	244
220	6.51	2.69	9.23			.59	.00	1.09	.64	.00	66	244
240	6.37	2.98	8.94			.47	.11	1.03	.48	.11	80	244
260	6.23	3.29	8.63	154	317	.77	.00	.96	.74	.00	97	233
280	6.09	3.64	8.28		211	.00	6.62	.86	.00	5.72	111	228
300	5.96	4.00	7.92	− 154	154	1.14	1.57	.77	.87	1.20	129	216
320	5.83	4.45	7.47		− 219	1.14	1.14	.62	.71	.71	140	208
340	5.71	5.01	6.91			.62	.62	.41	.25	.25	− 154	− 196
$l = 13°.4$												
20	8.06	.21	11.21			.65	.71	1.42	.92	1.01	+ 11	− 192
40	7.91	.43	10.99			.99	1.36	1.40	1.39	1.90	9	192
60	7.77	.64	10.78			.32	.84	1.37	.44	1.15	+ 2	194
80	7.62	.88	10.54			.27	1.51	1.33	.36	2.01	− 1	196
100	7.47	1.12	10.30			.71	1.30	1.31	.93	1.70	15	201
120	7.33	1.35	10.07			.76	.38	1.27	.97	.48	21	205
140	7.19	1.59	9.83			.37	.64	1.24	.46	.79	26	210
160	7.04	1.85	9.57			.82	.00	1.19	.98	.00	33	218
180	6.88	2.15	9.27			.24	.73	1.14	.27	.83	42	220
200	6.73	2.45	8.97			.46	.28	1.08	.50	.30	48	220
220	6.58	2.78	8.64			.68	.30	1.01	.69	.30	64	219
240	6.45	3.08	8.34			.64	1.23	.93	.59	1.14	81	214
260	6.32	3.42	8.00			.90	2.14	.84	.75	1.79	99	204
280	6.18	3.84	7.58			.00	5.67	.71	.00	4.03	113	194
300	6.05	4.33	7.09			1.32	1.32	.55	.72	.72	128	178
320	5.92	5.11	6.31			.65	.65	.25	.16	.16	− 143	− 160
$l = 15°.9$												
20	8.06	.22	10.68			.77	.00	1.40	1.08	.00	+ 11	− 187
40	7.92	.44	10.46	+ 125	− 240	.91	.81	1.37	1.25	1.11	10	187
60	7.78	.66	10.24	− 57	126	.76	.52	1.35	1.03	.70	+ 2	187
80	7.64	.89	10.01			.57	1.00	1.31	.75	1.31	− 1	190
100	7.50	1.13	9.77	25	208	.72	.80	1.27	.91	1.02	20	196
120	7.36	1.38	9.52			.81	.68	1.24	1.00	.84	23	198
140	7.23	1.62	9.28			.40	.00	1.19	.48	.00	29	198
160	7.09	1.89	9.01			.34	.00	1.14	.39	.00	33	199
180	6.94	2.20	8.70			.50	.00	1.07	.54	.00	42	199
200	6.79	2.53	8.37	73	185	.73	.00	1.00	.73	.00	44	198
220	6.65	2.87	8.03	177	141	1.24	.84	.91	1.13	.76	63	196
240	6.51	3.26	7.64	− 158	− 141	1.83	1.52	.79	1.45	1.21	84	187
260	6.39	3.65	7.25			1.05	2.23	.68	.71	1.51	101	176
280	6.26	4.18	6.72			.82	1.55	.49	.55	.55	− 116	− 162

TABLE 9 (*continued*)

f kc/s	R kpc	r_1 kpc	r_2 kpc	z_1 pc	z_2 pc	τ_1'	τ_2'	n_H/τ'	n_1 cm^{-3}	n_2 cm^{-3}	$\bar{z}_1$ pc	$\bar{z}_2$ pc
$l = 18°.4$												
20	8.07	.21	10.15			.93	.00	1.39	1.29	.00	+ 11	− 148
40	7.93	.44	9.92			1.33	1.79	1.35	1.80	2.42	9	150
60	7.80	.66	9.70			.69	.91	1.31	.90	1.19	+ 2	156
80	7.66	.91	9.45			.41	1.22	1.27	.52	1.55	− 2	165
100	7.53	1.15	9.21			.96	.05	1.23	1.18	.06	18	174
120	7.39	1.42	8.94			.71	.26	1.17	.83	.30	23	179
140	7.26	1.68	8.68			.46	.10	1.13	.52	.11	32	182
160	7.12	1.98	8.38			.42	.00	1.05	.44	.00	40	180
180	6.98	2.30	8.06			.40	.00	.98	.39	.00	47	176
200	6.84	2.66	7.70			1.00	.00	.88	.88	.00	50	167
220	6.70	3.07	7.29			.94	1.51	.76	.71	1.15	59	158
240	6.57	3.53	6.83			2.48	.40	.61	1.52	.24	70	136
260	6.45	4.11	6.25			3.21	3.21	.41	1.32	1.32	− 84	− 114
$l = 20°.9$												
20	8.07	.22	9.56			.86	.42	1.35	1.17	.57	+ 11	− 110
40	7.94	.45	9.33			1.14	1.62	1.30	1.48	2.11	9	113
60	7.81	.68	9.10	+ 9	− 150	.78	.18	1.26	.98	.23	+ 2	124
80	7.68	.93	8.85	− 88	202	.42	.19	1.21	.51	.23	− 3	140
100	7.55	1.19	8.59	+ 65	74	.61	.24	1.15	.70	.28	16	152
120	7.42	1.46	8.32	86	117	.60	.74	1.10	.66	.81	23	161
140	7.29	1.75	8.03	+ 8	180	.53	.28	1.03	.55	.29	35	165
160	7.16	2.07	7.71			.43	.00	.95	.41	.00	47	162
180	7.03	2.42	7.36	− 54	175	.56	.32	.86	.48	.27	53	154
200	6.89	2.85	6.93	− 13	− 268	.93	.00	.73	.68	.00	55	136
220	6.76	3.34	6.44			1.73	.00	.57	.98	.00	55	121
240	6.62	4.16	5.62			1.23	1.23	.28	.34	.34	− 57	− 85
$l = 23°.4$												
20	8.07	.24	8.96			.65	.06	1.31	.85	.08	+ 7	− 121
40	7.95	.46	8.74			1.33	.34	1.26	1.68	.43	+ 4	123
60	7.82	.72	8.48			.79	.30	1.21	.96	.36	− 1	128
80	7.70	.97	8.23			.46	.00	1.15	.53	.00	7	136
100	7.57	1.25	7.95			.76	.00	1.08	.82	.00	16	138
120	7.45	1.53	7.67			.59	.30	1.02	.60	.31	22	136
140	7.32	1.87	7.33			.59	.66	.93	.55	.61	31	138
160	7.20	2.21	6.99			.60	.72	.83	.50	.60	41	134
180	7.07	2.63	6.57			.40	1.50	.70	.28	1.05	59	126
200	6.93	3.21	5.99			1.31	.00	.51	.67	.00	62	99
220	6.80	4.23	4.97			.46	.46	.14	.06	.06	− 65	− 72
$l = 25°.9$												
20	8.08	.23	8.37		− 123	.16	1.45	1.25	.20	1.81	+ 2	− 132
40	7.96	.47	8.13			1.45	.00	1.20	1.74	.00	0	132
60	7.83	.75	7.85			1.08	.00	1.13	1.22	.00	− 4	132
80	7.71	1.03	7.57			.71	.00	1.07	.76	.00	11	132
100	7.59	1.32	7.28	− 7	20	.54	.27	.99	.53	.27	16	123
120	7.47	1.64	6.96	− 42	117	.72	.65	.90	.65	.58	21	113
140	7.35	2.00	6.60	+ 1	167	1.14	.40	.80	.91	.32	26	110
160	7.23	2.42	6.18	− 7	112	.78	.78	.67	.52	.52	34	108
180	7.10	3.00	5.60		− 6	.23	1.31	.47	.11	.62	− 66	− 99
$l = 28°.4$												
20	8.08	.26	7.74			.65	.38	1.16	.75	.44	− 9	− 132
40	7.96	.52	7.48			1.52	.10	1.11	1.69	.11	13	132
60	7.84	.81	7.19			1.56	.00	1.04	1.62	.00	19	132
80	7.72	1.11	6.89			1.14	.00	.96	1.08	.00	23	132
100	7.60	1.45	6.55			.34	.35	.86	.29	.30	28	126
120	7.48	1.84	6.16			.54	1.16	.74	.40	.86	29	99
140	7.37	2.25	5.75			1.26	.66	.61	.77	.40	33	86
160	7.25	2.86	5.14			.51	.51	.41	.21	.21	− 38	− 73

TABLE 9 (*continued*)

f kc/s	R kpc	r_1 kpc	r_2 kpc	z_1 pc	z_2 pc	τ_1'	τ_2'	n_H/τ'	n_1 cm^{-3}	n_2 cm^{-3}	$\bar{z}_1$ pc	$\bar{z}_2$ pc
$l = 30°.9$												
20	8.08	.28	7.08			.93	.00	1.09	1.01	.00	− 21	− 132
40	7.97	.55	6.81	− 33:	− 209	1.88	.16	1.02	1.92	.16	28	132
60	7.85	.87	6.49	114	152	1.59	.16	.93	1.48	.15	33	132
80	7.73	1.23	6.13	56	197	.96	.09	.83	.80	.07	35	132
100	7.62	1.60	5.76	20	141	.96	.82	.72	.69	.59	38	131
120	7.50	2.09	5.27	− 22	− 60	.80	.84	.56	.45	.47	37	86
140	7.38	2.82	4.54			.52	.52	.31	.16	.16	− 40	− 62
$l = 33°.4$												
20	8.09	.28	6.40			1.19	.29	1.01	1.20	.29	− 15	− 106
40	7.97	.62	6.06			1.20	1.40	.91	1.09	1.27	20	100
60	7.86	.96	5.72			1.81	.00	.81	1.47	.00	26	99
80	7.74	1.39	5.29			.76	.97	.68	.51	.65	29	95
100	7.63	1.89	4.79			.89	.03	.52	.46	.02	35	88
120	7.51	2.79	3.89			.30	.30	.20	.06	.06	− 42	− 55
$l = 35°.9$												
20	8.09	.31	5.75		− 132	1.49	1.77	.91	1.35	1.61	− 9	− 80
40	7.98	.66	5.40		198	3.01	.00	.80	2.41	.00	12	68
60	7.86	1.10	4.96	− 44	44	1.03	.63	.67	.69	.42	20	66
80	7.75	1.62	4.44		− 33	.15	1.04	.50	.07	.52	22	58
100	7.64	2.48	3.58			.17	.17	.20	.03	.03	− 32	− 46
$l = 38°.4$												
20	8.09	.36	5.00			1.20	2.98	.79	.95	2.35	+ 11	− 66
40	7.98	.78	4.58			3.47	.20	.66	2.27	.13	0	60
60	7.87	1.31	4.05			1.11	.00	.48	.53	.00	− 11	57
80	7.76	2.29	3.07			.20	.20	.14	.03	.03	− 30	− 44
$l = 40°.9$												
20	8.09	.43	4.17			.00	7.04	.64	.00	4.53	+ 11	− 57
40	7.98	.98	3.62			2.22	.00	.46	1.02	.00	0	47
60	7.88	1.90	2.70			.50	.50	.14	.07	.07	− 22	− 36

and WHITFORD [1]) located a number of O associations. The three associations with $l > 341°$ are all situated in a region where n_H exceeds 1.0. This *Sagittarius arm* may be followed to the other side of the Galactic System to at least $l = 357°$. Below $l = 357°$ the structure becomes quite complicated. It is interesting to note that in this region the height of the hydrogen layer shows evident irregularities (Figure 7). The arm may consist of two components at different z, but higher angular resolution is needed to solve this problem.

The next arm, seen tangentially at $l = 6°$, merges into the complicated region just described. Towards the sun it may be followed down to 4 kpc distance from the sun at $l = 355°$. Here it merges with another arm which runs mainly parallel to the previous arm. This arm is tangential to the line of sight at $l = 359°$. It does not seem to merge with the same arm at the other end. Finally, a not very dense arm may be seen tangentially at $l = 346°$.

KWEE, MULLER and WESTERHOUT [2]) found secondary maxima in their curve of rotational velocities, which they attributed to spiral arms seen tangentially at $l = 3°.4$ and $l = 18°.4$. These longitudes agree quite well with the arms found at $l = 6°$ and $l = 18°$ in the present investigation. Also, the secondary maximum of the rotational velocity at $l = 348°.4$ agrees with the arm found at $l = 346°$. Both the Orion arm and the Sagittarius arm clearly are inclined in the sense that they are trailing.

Plate B shows that the Orion and Sagittarius arms are denser in the regions which are more distant from the sun. Too large an *average* density in the far points would result if the assumed thickness of the hydrogen layer had been too large. Average hydrogen densities were computed for the near points and for the far points in two intervals of R. Table 8 shows that the differences in average densities of near and far points are not large.

The author wishes to thank Mr E. DE ROOY, who carried out most of the extensive calculations. Prof. VAN DE HULST kindly read the manuscript.

[1]) *Ap. J.* **118**, 318, 1953.
[2]) *B.A.N.* **12**, 211 (No. 458), 1954.